Exploiting the Greenland volcanic ash repository to date caldera-forming eruptions and widespread isochrons during the Holocene

Siwan M. Davies [a,*], Paul G. Albert [a,b], Anna J. Bourne [a,1], Sara Owen [a,2], Anders Svensson [c], Matthew S.M. Bolton [d], Eliza Cook [c], Britta J.L. Jensen [d], Gwydion Jones [a], Vera V. Ponomareva [e], Takehiko Suzuki [f]

[a] Department of Geography, Faculty of Science and Engineering, Swansea University, Singleton Park, Wales, SA2 8PP, UK
[b] School of Archaeology, University of Oxford, Oxford, OX1 3TG, UK
[c] Physics of Ice, Climate and Earth (PICE), Niels Bohr Institute, University of Copenhagen, Tagensvej 16, DK-2200, Copenhagen, Denmark
[d] Department of Earth and Atmospheric Sciences, University of Alberta, Edmonton, AB, T6G 2E3, Canada
[e] Institute of Volcanology and Seismology, Piip Boulevard 9, Petropavlovsk-Kamchatsky, 6830006, Russia
[f] Department of Geography, Tokyo Metropolitan University, Minamiosawa, Hachioji, Tokyo, Japan

ARTICLE INFO

ABSTRACT

Polar ice-cores have long been recognised as unrivalled repositories of past volcanic events. Although tephra products from local eruptions tend to dominate these records, improvements in micro-sampling and analytical techniques are uncovering a growing number of cryptotephras erupted from exceptionally distant volcanoes. We present a series of nine Middle Holocene cryptotephra deposits detected within the NGRIP ice-core that originate from five different volcanic regions across the Northern Hemisphere (Alaska, Cascades, Iceland, Japan, Kamchatka). Unique compositional signatures are employed to identify ash from three large caldera-forming events in Kamchatka (KS_2 from Ksudach), the Cascades (Mazama) and North East Japan (Mashu), along with ash from the Hekla 4 eruption in Iceland. High-precision ice-core ages (adopting a 1950 CE datum for the GICC05 timescale assigned to the Greenland ice cores) are derived for each eruption: Hekla 4 (4325 ± 8 a b1.95k), KS_2 (7089 ± 26 a b1.95k), Mashu (i-f) (7473 ± 33 a b1.95k) and Mazama (7562 ± 35 a b1.95k), all of which can be employed as chronological fix-points in other proxy records where these deposits are also preserved. Four further cryptotephra deposits and one macro-deposit are also identified and traced to sources in Iceland and Alaska. The cryptotephra originating from Alaska is correlated to a deposit identified in lake records from the Kenai Peninsula, thought to originate from Redoubt Volcano. The remaining four deposits are typical of the products of Katla, Grímsvötn and Veiðivötn in Iceland. This ensemble of Middle Holocene tephra deposits highlights the pivotal position of the Greenland ice-sheet and its ice-cores to capture deposition from the convergence of several far-travelled ash clouds. Precise age estimates derived from the annually resolved ice-core record greatly enhances the value of these tephra isochrons.

1. Introduction: the Greenland tephra repository

Polar ice-cores have long been recognised as valuable repositories of volcanic activity. Volcanic products such as ash particles (tephra) and sulphate aerosols are dispersed via the atmosphere, deposited instantaneously (in geological terms) on the ice surface, buried by subsequent snowfall, and sealed and preserved within the ice. This mode of deposition, along with the geochemical source fingerprint, locked within the ash particles, gives rise to isochrons or marker horizons that can be employed for reconstructing volcanic histories and for correlating a wide range of proxy archives. Although synchronised aerosol records from both poles can give rise to detailed records of large global eruptive events (e.g. Sigl et al., 2015; Svensson et al., 2020; Lin et al., 2022), only the geochemical fingerprint of the ash particles can provide an

unambiguous method for identifying the volcanic source and the specific eruption (e.g. Bourne et al., 2016; McConnell et al., 2020; Smith et al., 2020; Plunkett et al., 2023). Ash particles trapped within the ice, therefore, represent an unrivalled and, to some extent, untapped potential to build a global record of volcanism (Self and Gertisser, 2015).

Initial exploration of the ash content in Greenland ice was drawn to the well-preserved visible horizons or where large peaks in electrical conductivity measurements and sulphate were observed (Palais et al., 1991; Grönvold et al., 1995; Zielinski et al., 1997). This targeted sampling approach led to the identification of a handful of volcanic deposits such as the North Atlantic Ash Zone II (NAAZII) and Vedde Ash in pre-Holocene ice (Grönvold et al., 1995; Zielinski et al., 1997), the Saksunarvatn Ash and Mazama in Holocene ice (Grönvold et al., 1995; Zdanowicz et al., 1999), along with historical events such as Oræfajökull 1362 CE (Palais et al., 1991), Eldgjá 939–940 CE (Zielinski, 1995) and Landnám 871 (Grönvold et al., 1995). More recently, Greenland ice-core records have been scoured for microscopic traces of ash particles (so-called cryptotephras) (e.g. Mortensen et al., 2005; Davies et al., 2010; Abbott et al., 2012; Coulter et al., 2012; Davies et al., 2014; Bourne et al., 2015; Cook et al., 2018, 2022; Plunkett et al., 2023). As a result, a new catalogue of volcanic events has emerged spanning the last 123,000 years filling important knowledge gaps in the timing and frequency of volcanic events and giving rise to new chrono-stratigraphic marker horizons that were hitherto unattainable. Despite the new level of detail uncovered within this repository, the products of local Icelandic eruptions typically dominate (Bourne et al., 2015; Cook et al., 2022). Although such local deposits are valuable as regional isochrons for correlation, uncovering ash from more distal sources is an important step towards building a source-constrained hemispheric to global volcanic record, while in turn widening the geographical areas over which correlations are possible and complementing the existing volcano climate-forcing indices (Toohey and Sigl, 2017; Sigl et al., 2022).

In the early days of ice exploration, traces of low-latitude eruptions were reported by a small number of studies (Palais et al., 1992; De Silva and Zielinski, 1998), but the challenges of extracting robust and replicable geochemical data from a few microscopic particles have always plagued this work. However, improvements in micro-analysis (namely, microprobe beam size reduction, Hayward (2012)) and modifications to sample preparation have facilitated a new focus. Volcanic events during the Common Era from Alaska, Asia and Central America have been chronicled by Jensen et al. (2014), Sun et al. (2014), Smith et al. (2020) and Plunkett et al. (2023), whereas Bourne et al. (2016) identified a series of silicic eruptions in last glacial ice originating from the Pacific Arc volcanoes. In contrast, very few volcanic events have been reported in Greenland ice from the Early and Middle Holocene periods (e.g. Cook et al., 2018). Here, we present new data to fill the gap during the Early and Middle Holocene period that demonstrate how Greenland is a critical linchpin and repository for capturing ash originating from several distal volcanic centres across the northern hemisphere. Our findings provide evidence of ash dispersal over 7000 km from the volcanic source to deposition on the Greenland ice sheet. Volcanic glass shards originating from several well-documented eruptions are uncovered, including three Middle Holocene caldera-forming eruptions from the circum-Pacific region, as well as ash from the Hekla 4 eruption (Iceland), a widely used isochron for correlation of Northern European sediment records. Our discoveries also include the lesser-known eruption of the Mashu volcano in Hokkaido, Japan, previously thought to have resulted in only local/regional ashfall distribution (e.g. Razzhigaeva et al., 2016). Geochemical analyses of single-glass shards are employed to pinpoint the source of each deposit and we assign the best available ages based on their stratigraphic position within the annually resolved ice-core record.

2. Methods

2.1. Sample selection and tephra analysis

Three main time intervals during the Early to Middle Holocene were sampled from the NGRIP ice-core (75.1° N, 42.3°W). These intervals were selected according to the likely timing of well-known major volcanic events or widely dispersed distal tephra in the northern hemisphere (Table 1). The main sampling intervals were as follows: Interval 1) 8300–8600 a b2k in a bid to identify KO tephra related to the Kurile Lake caldera (Kamchatka); Interval 2) 6500–7700 a b2k to search for tephras such as KS_2 (Ksudach, Kamchatka) and Kikai-Akahoya (K-Ah, Japan), and Interval 3) 4300–4400 a b2k to pinpoint the Hekla 4 deposit (Fig. 1; Table 1). Seven targeted windows were also investigated within a fourth interval in a search for Late Holocene tephras that are widespread isochrons in northern Europe e.g. Glen Garry and Hekla 3 (labelled Interval 4 on Fig. 1). In addition to the NGRIP samples, a 1 mm thick deposit within the 6500–7700 a b2k interval in GRIP ice, observed during a different sampling campaign, was also included in this study. Additional Holocene time-intervals and ice-cores are being investigated as part of other ongoing studies (e.g. Cook et al. unpublished).

Ice cores archived at the University of Copenhagen were sampled into 20, 15 or 11 cm long samples, typically providing an annual to sub-annual resolution during this interval (Fig. S1, Supplementary Information 3). Where volcanic glass shards were identified with optical microscopy, ice was re-sampled at higher resolution to constrain the stratigraphic position and age of selected tephra to a 5–10 cm interval. In total, 214.65 m of ice was sampled, amounting to 1207 individual samples. Samples were melted and centrifuged, and the supernatant was discarded. The remaining sample was mounted onto frosted glass slides and embedded in epoxy resin (e.g. Bourne et al., 2015).

2.2. Tephra identification and geochemical analysis

Optical microscopy was employed to identify the presence of volcanic glass shard particles and to identify samples for geochemical analysis. Long axis data for single grains were measured either using a Scanning Electron Microscope or an optical microscope (Table 2, Fig. S2, Supplementary Information 4). Unique labels are assigned to each tephra deposit based on the ice-core name and the lowermost depth of the sample. For example, a tephra found in the NGRIP record between 751.95 and 752.05 m is assigned a label of NGRIP 752.05 m (Table 2). For each identified tephra two age estimates are reported in Table 2: GICC05 ages relative to the year 2000 CE (b2k) and GICC05 ages relative to 1950 CE (b1.95k). The latter ages are also corrected according to the recommendations of Adolphi and Muscheler (2016) (Table 2). Maximum counting uncertainties for the GICC05 ages are typically considered to be 2 sigma uncertainties (Andersen et al., 2006). In the main body of the manuscript, ages for the ice-core tephras are reported as GICC05 ages relative to the 1950 CE datum (GICC05 a b1.95k) to facilitate comparisons with ages derived by other chronological methods such as radiocarbon dating.

Samples containing tephra were ground and polished using silicon carbide paper and 6, 3 and 1 μm diamond suspension. Major element analysis for the ice-core deposits was conducted by electron microprobe (EPMA) during two separate analytical periods at the Tephra Analysis Unit, University of Edinburgh. Ten major and minor elements were analysed from single shards on a Cameca SX-100 instrument equipped with five vertical wavelength dispersive spectrometers with an accelerating voltage of 15 kV, beam diameter of 5 or 3 μm and beam current of 0.5, 2 and 80 nA (depending on the beam diameter used) (Supplementary Information 1). All data are normalised and presented visually on an anhydrous basis, with full data-sets available in Supplementary Information 1. Major element data for comparative reference samples, for Mazama, Mashu and UA 2960, reported for the first time here and analysed on the Edinburgh, Oxford and Alberta microprobes, are also

Table 1

Summary of the targeted eruptions and/or widely traced distal tephra deposits from volcanic sources in the Northern Hemisphere. The majority of the target eruptions have a volcanic explosivity index (VEI) of ≥5. Distally known tephra deposits (distal) with uncertain sources (labelled with #) are assumed to be VEI ≥4. Age estimates are given in cal a BP (unless stated) with 2 sigma uncertainties; * are ^{14}C age estimates that are re-calibrated in this study with IntCal20 (Reimer et al., 2020) and the original ^{14}C age is also given, † denotes an age range derived from varve records and ‡ is an ice-core age. Hekla 5 and Lairg A have been suggested to be the same event and it is also uncertain whether the Lairg B and the Hoy tephra are the same or separate events (Plunkett and Pilcher, 2018). The [superscript numbers] reported with the tephra volume, VEI and eruption/tephra deposit refer to the original references. References are numbered as follows: 1 Melekestsev et al. (1998), 2 Ponomareva et al. (2004), 3 Buckland et al. (2020), 4 Egan et al. (2015), 5 Zdanowicz et al. (1999), 6 Braitseva et al. (1997), 7 MacLeod et al. (1995), 8 Jensen et al. (2021), 9 Machida and Arai (2003), 10 Smith et al. (2013), 11 Ponomareva et al. (2017), 12 Larsen and Thorarinsson (1977), 13 Global Volcanism Program (2023), 14 Thorarinsson (1971), 15 Walsh et al. (2021), 16 Pilcher et al. (1996), 17 Dugmore et al. (1995b), 18 Dörfler et al. (2012), 19 Stevenson et al. (2015), 20 Dugmore et al. (1995a), 21 Zillén et al. (2002), 22 Walsh et al. (2023), 23 Plunkett et al. (2004), 24 Martin-Puertas et al. (2021), 25 Barber et al. (2008), 26 Dräger et al. (2016), 27 Gudmundsdóttir et al. (2016).

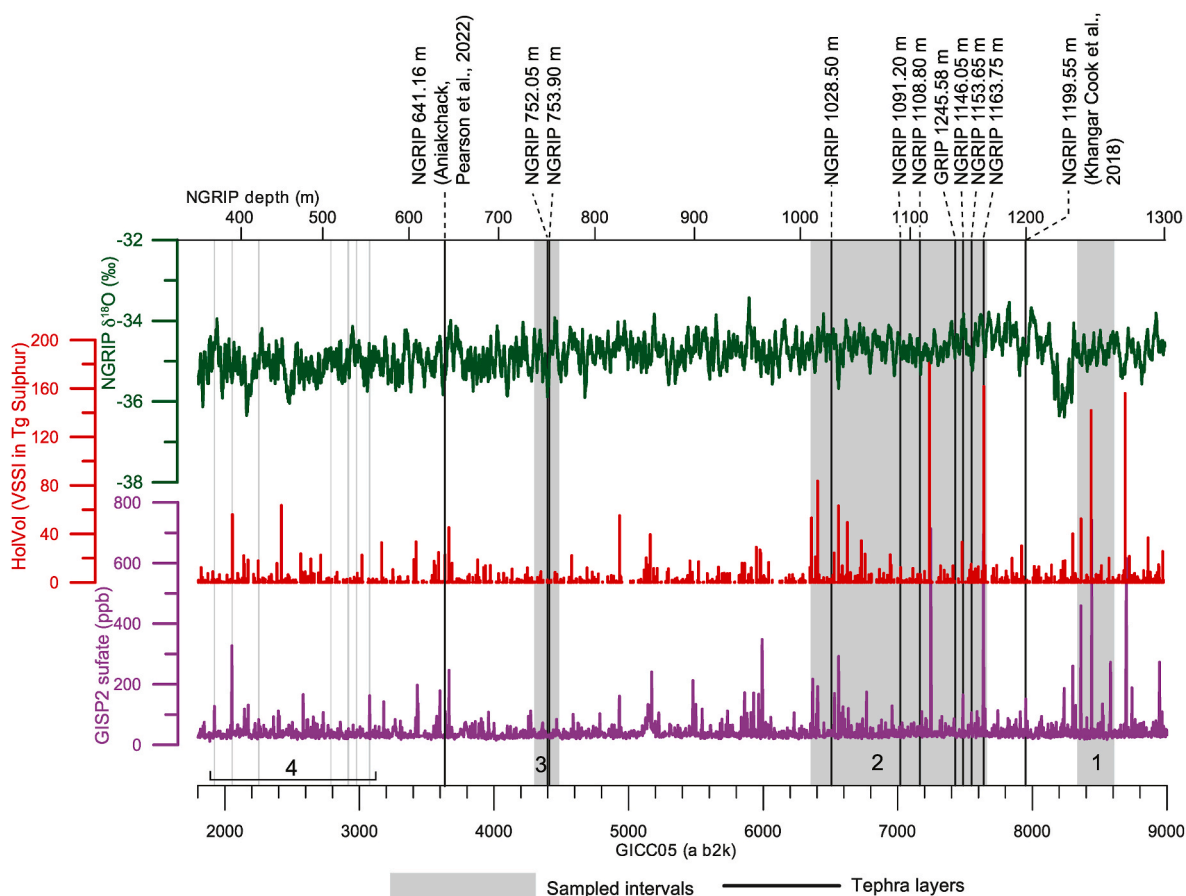| Volcanic source	Eruption/Tephra deposit	Region	Glass Composition (TAS)	Tephra volume (km^3)	VEI	Age (cal a BP, unless stated)	Original ^{14}C age (if re-calibrated)	Age references
PACIFIC ARC								
Kurile Lake	KO	Kamchatka, Russia	Rhyodacite-andesite	140–170 [1]	7 [2]	8515–8380*	7618 ± 14	2
Mount Mazama (Crater Lake)	Mazama	Oregon, USA	Rhyolite	~176 [3]	7 [5]	7682–7584		4
						7627 ± 150‡		5
Kizimen (KZ)	KZ	Kamchatka, Russia	Dacite	2.5–3 [6]	5[13]	8410–8205*	7531 ± 37	6
Newberry	East Lake	Oregon, USA	Rhyolite	–	–	7835–6945*	6400 ± 130	7
						7280–6835		8
						7430–6555		8
Kikai (K)	Akahoya (K-Ah)	S. Kyushu, Japan	Rhyolite	150 [9]	7 [9]	7303–7165		10
Ksudach (KS)	KS$_2$	Kamchatka, Russia	Andesite-Rhyolite	8.9–10.5 [8]	5 [8]	7245–6795*	6007 ± 38	6
						6877–6693		11
						7185–6970		8
ICELAND								
Hekla	Hekla 5 (H5)/Lairg A (distal)	Iceland	Basalt to Rhyolite	3 [12]	5[13]	7310–6795*	6185 ± 100	14
						7240–7100†		15
						6998–6809 (Lairg A)		16
Torfajökull (#)	Lairg B (distal)/Hoy (distal)	Iceland		–	–	6728–6564 (Lairg B)		16
						6600–6125* (Hoy)	5560 ± 90	17
						6832–6615† (Lairg B)		18
Hekla	Hekla 4 (H4)	Iceland	Basalt to Rhyolite	11.2 [19]	5[13]	4283–4153*	3826 ± 12	20
						4345–4229		16
						4417–4266†		18
						4497–4283†		21
						4467–4403†		22
Hekla	Hekla 3 (H3)	Iceland	Dacite-Rhyolite	13.3 [19]	5[13]	3150–2875*	2879 ± 34	20
						3068–3120†		18
						3390–3200†		21
Vatnajökull (#)	Microlite/OMH-185 (distal)	Iceland	Rhyolite	–	–	2705–2630		23
						2646–2588†		24
Askja (#)	Glen Garry (distal)/A2000 [27]	Iceland	Rhyolite			2210–1966		25
						2280–2060†		26
						2112–2034†		24

Fig. 1. NGRIP and GRIP ice-core tephra deposits plotted against the NGRIP oxygen isotope record (NGRIP members, 2004; Vinther et al., 2006), GISP2 sulphate data (Mayewski et al., 1997) and Holocene volcanic stratospheric sulphur injection events (Sigl et al., 2022) reconstructed from synchronisation of bipolar events. All ice-core data are plotted on the GICC05 timescale (b2k: before year 2000 CE) and synchronised using the same approach as Veres et al. (2013). The stratigraphic position of the Khangar Tephra identified by Cook et al. (2018) and the Aniakchak Tephra reported by Coulter et al. (2012) and Pearson et al. (2022) are also shown. Sampled intervals (labelled 1–4) are shown by grey shading. No glass shards were identified in the targeted sampling within Interval 4 < 600 m depth.

presented in Supplementary Information 1 and 2 alongside full details of the operating conditions.

Trace element analyses were conducted on volcanic glass shards extracted from three of the NGRIP ice samples (NGRIP 1108.80 m, 1153.65 m and 1163.75 m). These samples were selected for trace element analysis in order to test and support a correlation to events from Pacific Arc volcanoes. Additionally, reference glasses of near-source eruption deposits (pumice and ash) from caldera-forming eruptions at Crater Lake (Cascades, USA) and Mashu (Hokkaido, Japan) were also analysed. Trace element analyses were performed using an Agilent 8900 triple quadrupole ICP-MS (ICP QQQ) coupled to a Resonetics 193 nm ArF excimer laser-ablation in the Department of Earth Sciences, Royal Holloway, University of London. Full analytical procedures adopted here follow Tomlinson et al. (2010) and details are provided in Supplementary Information 1.

3. Results

Nine tephra deposits were identified and geochemically analysed (Table 2 and Fig. 1). Eight were cryptotephra in form (i.e. no discernible deposit observed in the ice with the naked eye). Seven deposits were identified in Interval 2 (6500–7700 a b2k; 1009.80–1166.55 m), and two deposits in Interval 3 (4300–4400 a b2k; 738.10–763.95 m) (Fig. 1). No glass shards were found in Interval 1 (8300–8600 a b2k; 1238.60–1265.00 m) or the targeted windows in Interval 4 (Fig. 1). Particles that resemble volcanic glass shards were observed in NGRIP 1111.55–1111.75 m (Interval 2), but geochemical analyses proved

elusive due to problems during slide polishing, despite several re-sampling attempts. Geochemical analysis of two small potential tephra shards in NGRIP 509.85–509.96 m (Interval 4) revealed that they were not volcanic glass.

Shard concentrations and particle size (maximum length or long axis) vary significantly between samples (Table 2). The highest shard concentration for the cryptotephra deposits is recorded in NGRIP 1153.65 m (>5000 shards). Shards in this sample are typically platy in morphology (Fig. 2) with long axes ranging between 5 and 126 μm with a mode of 10–20 μm (Table 2, Fig. S2, Supplementary Information 3 and 4). Over 1000 shards were identified in NGRIP 1163.75 m with all other deposits revealing abundances in the hundreds or tens of shards (Table 2). Glass shards from NGRIP 752.05 m and NGRIP 1153.65 m are particularly fine-grained with 86% and 66% of grains measured being ≤20 μm (maximum length) (Table 2, Fig. 2, Fig. S2, Supplementary Information 3 and 4).

Three deposits are rhyolitic in composition (NGRIP 1163.75 m, NGRIP 1153.65 m and NGRIP 1028.50 m), with three exhibiting a basaltic composition (NGRIP 1146.05 m, GRIP 1245.58 m and NGRIP 1091.20 m) (Fig. 3). The remaining three deposits reveal evolutionary trends or bimodal compositions (NGRIP 1108.80 m, NGRIP 753.90 m and NGRIP 752.05 m) (Table 2; Fig. 3). Geochemical signatures indicate that five deposits originate from Iceland and four correlate to circum-Pacific arc volcanic sources. The diagnostic features and proposed correlations to volcanic sources are presented according to their source region below.

Table 2
Summary of tephra deposits identified in the NGRIP and GRIP ice cores. Full depth range for each tephra sample is provided, and the lowermost depth is used as the label for each tephra in the main text. GICC05 ages are from Vinther et al. (2006) and presented with 2000 CE (b2k) as the datum; age uncertainties are given as maximum counting error (MCE), typically considered to be equivalent to 2 sigma uncertainties. GICC05 ages are also presented by using 1950 CE as the datum (b1.95k) and include the correction recommended by Adolphi and Muscheler (2016). The GICC05 a b1.95k ages are used in the main text. Compositional characterisation is based on Le Maitre (1989) and Jakobsson et al. (2008). Long axis measurements (min-max) of the glass shards in each sample are reported (full data-set provided in Supplementary Information 4).

Sample	Age (GICC05 a b2k)	Age (GICC05 a b1.95k)	Shards (n)	Long axis (Min-Max) (μm)	Composition	Source	Tephra correlation	Shards analysed for major elements (n)	Shards analysed for trace elements (n)
NGRIP 751.95–752.05	4397 ± 8	4325 ± 8	141	3–37	Rhyolite/transitional rhyolite	Hekla	Hekla 4	9	–
NGRIP 753.85–753.90	4411 ± 8	4338 ± 8	203	12–74	Bimodal: Transitional Basalt & transitional trachyte	Katla	Dacite: Katla SILK Basalt: Unknown	33	–
NGRIP 1028.35–1028.50	6508 ± 19	6430 ± 19	41	15–20	Rhyolite	Redoubt	Redoubt (UA 2960)	8	–
NGRIP 1091.05–1091.20	7019 ± 23	6943 ± 23	16	20–50	Transitional Basalt	Katla	Unknown	5	–
NGRIP 1108.75–1108.80	7164 ± 26	7089 ± 26	77	6–13	Andesite-Rhyolite	Ksudach	KS_2	16	5
GRIP 1245.57–1245.58	7428 ± 32	7353 ± 32	Visible	20–35	Transitional Basalt	Grimsvötn/Hekla	Unknown	24	–
NGRIP 1145.85–1146.05	7485 ± 32	7410 ± 32	217	20–30	Tholeiitic Basalt	Veiðivötn	Unknown	20	–
NGRIP 1153.55–1153.65	7548 ± 33	7473 ± 33	>5000	5–126	Rhyolite	Mashu	Mashu i-f	30	8
NGRIP 1163.70–1163.75	7637 ± 35	7562 ± 35	1200	10–80	Rhyolite	Crater Lake	Mazama	18	14

3.1. Tephra deposits originating from circum-Pacific arc volcanism

Three Middle Holocene cryptotephra deposits, NGRIP 1108.80 m, 1153.65 m, and 1163.75 m, exhibit mantle-normalised trace element profiles diagnostic of subduction-related volcanism (Fig. 4B), and differ from the typical signature of products from the divergent tectonic setting in Iceland, the dominant source of tephra in the Greenland ice cores (e.g. Bourne et al., 2016). Diagnostic features of arc volcanism include enrichment in the large ion lithophile elements (e.g. Rb to Ba) relative to the high field strength elements (HFSE; e.g. Nb, Ta) and the rare earth elements (REE; i.e. La to Lu), and pronounced depletions at Nb and Ta (Fig. 4B). In addition, these three subduction-related tephra layers display tholeiitic (low-K) through to calc-alkaline (medium-K) volcanic glass affinities (Figs. 3 and 4), which is consistent with circum-Pacific arc volcanism, and in particular volcanic sources along the Japanese, Kurile, Aleutian and Cascade arcs (e.g. Bourne et al., 2016; Portnyagin et al., 2020). We consider the chemical signature of these deposits in the context of known large-magnitude explosive eruptions at circum-Pacific arc volcanoes during the Middle Holocene (Crosweller et al., 2012).

Only major element data were obtained for NGRIP 1028.50 m, thus we cannot consider the tectonic setting in the same way as for the other three tephras from the circum-Pacific Arc volcanoes. However, based on the major element data available, we suggest a potential Pacific Arc volcanic source and tephra correlative.

3.1.1. NGRIP 1163.75 m: Mazama tephra

NGRIP 1163.75 m, dated at 7562 ± 35 a b1.95k, displays a homogenous rhyolitic (73.35 ± 0.22 wt% SiO_2) glass composition with a calc-alkaline affinity (2.78 ± 0.06 wt% K_2O) (Fig. 3). Trace element concentrations are also largely homogeneous (e.g. 241 ± 23 ppm Zr; 6.7 ± 0.7 ppm Nb), with enrichment in light REE relative to heavy REE (La/Yb = 8.6 ± 0.2) and constant incompatible trace element ratios (e.g. Zr/Th = 47.8 ± 6.2; Nb/Th = 1.3 ± 0.2). This chemical signature is consistent with deposits of the caldera-forming Mount Mazama eruption in Oregon, which formed the modern-day Crater Lake (Fig. 4). Initial Plinian activity at Mount Mazama preceded caldera-collapse, which produced large volume pyroclastic density currents (PDC; Bacon, 1983; Young, 1990). Volume estimates suggest ~61 km³ Dense Rock Equivalent (DRE) was erupted, equating to a Magnitude 7.1 eruption according to the Pyle (2000) classification (Buckland et al., 2020). Tephra fall from the eruption was predominantly dispersed towards the northeast, forming a visible macro-tephra across the western USA and Canada (Buckland et al., 2020), and preserved as a cryptotephra in sediments from Lake Superior (Spano et al., 2017), Newfoundland (Pyne-O'-Donnell et al., 2012), and in nearby Placentia Bay (Monteath et al., 2023).

The Mazama tephra was previously identified in the GISP2 ice-core retrieved from the Greenland Summit and relates to a prominent sulphate peak dated to 7627 ± 150 cal a BP (Zdanowicz et al., 1999). Chemo-stratigraphic matching of the Greenland and Antarctic ice-cores (Sigl et al., 2022), along with the tephra geochemical data support the firm correlation of NGRIP 1163.75 m to the Mazama caldera-forming eruption.

3.1.2. NGRIP 1153.65 m: Mashu i-f tephra

The two low-K arc derived cryptotephra deposits, NGRIP 1153.65 m and NGRIP 1108.80 m, show low Rb values (15.5 ± 3.0 ppm and 19.6 ± 8.4 ppm, respectively) and flat REE profiles (Fig. 4), indicative of forearc eruptive products. Such chemical features are characteristic of volcanic sources along the northeastern Japan Arc and the Kurile Arc (Ponomareva et al., 2017; Albert et al., 2019). Constrained to 7473 ± 33 a b1.95k, NGRIP 1153.65 m exhibits a dominant rhyolitic population where SiO_2 ranges between 71.27 and 74.02 wt% (n = 27 shards) (Fig. 3). Three shards are dacitic in composition with SiO_2 values of <70 wt% (Fig. 3). A distinctive feature of all glass shards is low K_2O values
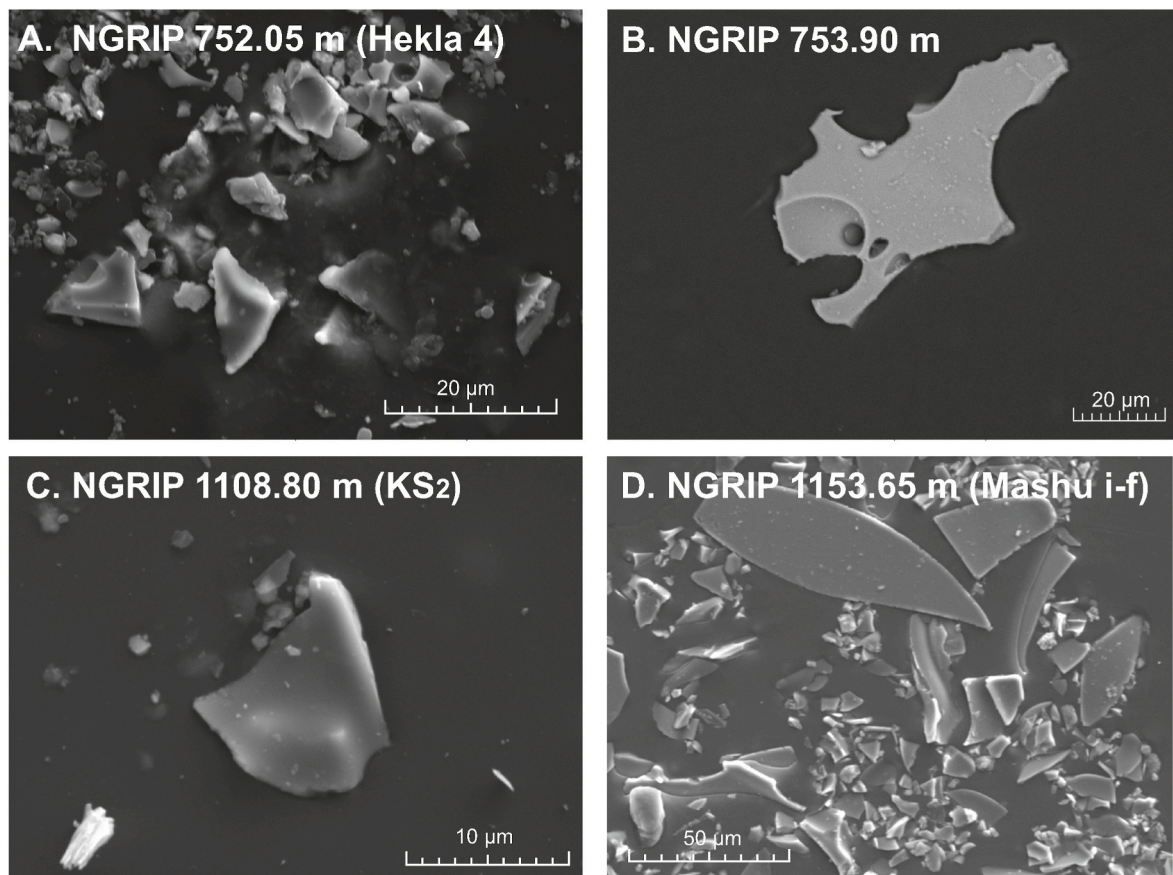
Fig. 2. Scanning Electron Microscope images of selected NGRIP tephra glass shards from **A.** NGRIP 752.05 m, **B.** NGRIP 753.90 m, **C.** NGRIP 1108.80 m, **D.** NGRIP 1153.65 m.

(0.53–0.83 wt%) (Figs. 3 and 4 and Supplementary Information 1). Enrichment in incompatible trace elements is also particularly low (e.g. Zr 103 $\pm$ 9 ppm; Th 1.2 $\pm$ 0.2 ppm), while the ratios are relatively constant (e.g. Zr/Th = 83.5 $\pm$ 9.2), and there is no enrichment in the light REE relative to the heavy REE (La/Yb = 1.6 $\pm$ 0.4).

Low alkaline products are diagnostic of Japanese sources and the chemical signature for NGRIP 1153.65 m is entirely consistent with the distinctly low-K eruptive products of the Mashu volcano, located on the rim of the Kutcharo caldera (NE Hokkaido Island), one of the most productive Holocene volcanoes in Japan (Kishimoto et al., 2009). The low-K Mashu products are distinguishable from the other post-caldera Kutcharo centres (e.g. Atosanupuri and Nakajima) and the nearby Akan caldera that typically produce medium-K deposits (e.g. Hasegawa et al., 2012; Razzhigaeva et al., 2016). The Mashu (Ma) caldera was formed during the Middle Holocene, where the eruptive activity is categorised as VEI 6. The eruption is characterised by three Plinian fall units (Ma i-g) capped by a thick pyroclastic density current (PDC) deposit (Ma-f), which is thought to be associated with caldera-collapse (Kishimoto et al., 2009; Yamamoto et al., 2010; Hasegawa et al., 2012; Razzhigaeva et al., 2016). Our NGRIP 1153.65 m major and trace element results are consistent with new and previously published geochemical data-sets for the proximal low-K Mashu i-f deposits (Razzhigaeva et al., 2016; Albert et al., 2019) (Fig. 4). A correlation of NGRIP 1153.65 m to a specific eruptive phase (fall vs PDC) is not possible based on overlapping compositional signatures, and as such, we assign a correlation to Mashu i-f.

3.1.3. NGRIP 1108.80 m: KS2 tephra from Ksudach volcano

NGRIP 1108.80 m, dated at 7089 $\pm$ 26 a b1.95k, displays a broad andesitic to rhyolite evolutionary trend (SiO$_2$ 59.87–72.45 wt%) where

the majority of the shards are dacitic in composition (Fig. 3). CaO values extend between 2.68 and 7.54 wt% (Fig. 4A), FeO$_t$ range from 3.44 to 10.19 wt% and K$_2$O concentrations are all <1.39 wt% (Fig. 3B). While this deposit is classified as a low-K (tholeiitic) tephra, it does reside at the calc-alkaline boundary on the SiO$_2$ vs K$_2$O classification diagram (Fig. 3B). Levels of incompatible trace elements in the NGRIP 1108.80 m glasses analysed are low (e.g. 105 $\pm$ 27 ppm Zr; 1.9 $\pm$ 0.6 ppm Nb; 0.9 $\pm$ 0.3 ppm Th), and, similarly to NGRIP 1153.65 m, there is no enrichment in the light REE relative to the heavy REE (La/Yb = 1.8 $\pm$ 0.3) (Fig. 4).

These glass shard compositions are consistent with the low K$_2$O glasses typically produced by Ksudach volcano (Braitseva et al., 1997; Volynets et al., 1999). Kamchatkan volcanic products are typically classified according to their K$_2$O values, with low K$_2$O products known to originate from volcanic sources in the frontal/coastal region close to the Kurile-Kamchatkan trench (e.g. Braitseva et al., 1997; Kyle et al., 2011; Portnyagin et al., 2020). Ksudach volcano is one of these sources and is known to have experienced multiple Holocene caldera-forming eruptions, including the couplet of explosive eruptions KS$_3$ and KS$_2$, the latter of which led to the formation of caldera IV in the Middle Holocene (Braitseva et al., 1995). The initial smaller volume KS$_3$ tephra deposit has a limited ash dispersal to the west, while the significantly more voluminous KS$_2$ tephra is linked with a caldera-collapse and tephra dispersal towards the north, giving rise to an important Middle Holocene marker horizon for the Kamchatkan Peninsula (Braitseva et al., 1997; Kyle et al., 2011; Plunkett et al., 2015; Ponomareva et al., 2017). An estimated tephra volume of 8.9–10.5 km^3 was produced during KS$_2$, with evidence of ultra-distal ash dispersal as far as Nova Scotia, Canada (Jensen et al., 2021), and the High Arctic in Svalbard, Norway (van der Bilt et al., 2017).
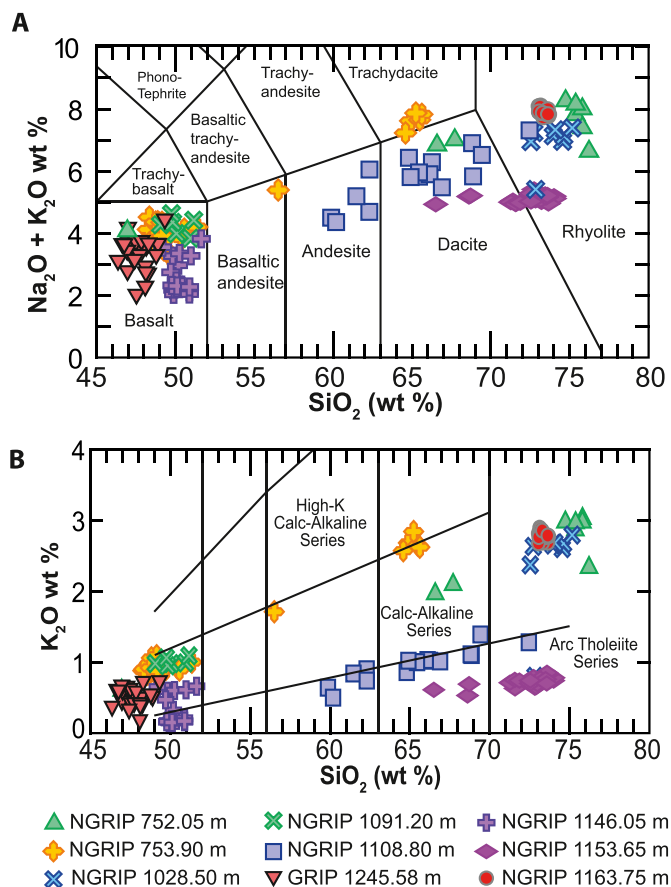
Fig. 3. A. Total alkali silica diagram for all NGRIP and GRIP tephras. Compositional classifications are based on Le Maitre (1989). **B.** SiO_2 vs K_2O classification diagram for all tephras presented (Peccerillo and Taylor, 1976).

Glass shard analyses from NGRIP 1108.80 m indicate a very strong correlation to near-source major and trace element compositions of both the KS_3 and KS_2 eruption units, which are chemically indistinguishable (Fig. 4). However, given the northwards dispersal trajectory and widespread extent of ash fallout, we attribute NGRIP 1108.80 m to KS_2 and provide a much-needed precise age estimate of 7089 ± 26 a b1.95k for this caldera-forming event (see section 4).

3.1.4. NGRIP 1028.50 m: Redoubt tephra

Major element analyses were obtained from eight single shards from NGRIP 1028.50 m. Two shards are considered to be outliers with CaO values greater than 3.0 wt%, compared to a mean of 2.0 wt% for the main population. These outliers are excluded in our pursuit of a correlation. Dated to 6430 ± 19 a b1.95k, NGRIP 1028.50 m is chemically inconsistent with any known silicic Icelandic eruptions that fall within the 6000–7000 year interval, such as the Lairg and Hoy tephras (Plunkett and Pilcher, 2018), Hekla Ö (Gudmundsdóttir et al., 2011b), and the newly discovered tephras identified in Diss Mere (Walsh et al., 2021).

However, the main population of NGRIP 1028.50 m plots within the field of known tephras from Redoubt Volcano, Alaska (see Fig. 5; Bolton et al., 2020). Redoubt has erupted many times during the Holocene, with multiple tephra deposits identified in lakes around SW Alaska (e.g. Riehle, 1985; Schiff et al., 2010). In particular, NGRIP 1028.50 m shards show a compositional affinity with a Middle Holocene tephra from Tustumena Lake (UA 2960) on the Kenai Peninsula (de Fontaine et al., 2007), as well as the oldest Redoubt tephra reported from Eklutna Lake (Tephra 19, UA 3074, Bolton et al., 2020) (Fig. 5). Furthermore, these tephras may also be related to the "Oshetna" tephra found across the southern interior of Alaska and dated to *ca.* 7930–6570 cal a BP

(Bigelow et al., 2019). The name "Oshetna" was applied to what was assumed to be a single tephra found across multiple archaeological sites and lake cores (e.g. Dixon, 1985; Dixon and Smith, 1990; Child et al., 1998). However, a detailed geochemical examination of the "Oshetna" tephra from numerous sites shows that it is characterized by at least four populations that appear to represent multiple tephra deposits (e.g. Mulliken, 2016; Bigelow et al., 2019, see Fig. 5A). One of the prominent "Oshetna" geochemical populations is attributable to Redoubt and plots with NGRIP 1028.50 m, UA 2960, UA 3074, as well as, with AT-3434, a tephra from Big Lake, Alaska, which includes the Redoubt population and a dacitic population that is also prominent in terrestrial "Oshetna" samples from the Middle Susitna Valley, Alaska (Fig. 5) (Bigelow et al., 2019).

Here, we updated the Tustumena Lake age-depth model of de Fontaine et al. (2007) as a P_Sequence deposition model (Bronk Ramsey, 2008; Ramsey and Lee, 2013) with radiocarbon ages calibrated using the IntCal20 curve (Reimer et al., 2020). This gives an age estimate of *ca.* 6500 cal a BP for UA 2960 (Fig. S3, Supplementary Information 3), with a 95.4% range between 7187 and 5864 cal a BP. Similarly, a revised age-depth model for Big Lake indicates that tephra AT-3434 was deposited *ca.* 6400 cal a BP (95.4% range between 7560 and 5087 cal a BP). Despite the broad range, these ages are consistent at the 95% level with the 6430 ± 19 a b1.95k age of the NGRIP 1028.50 m deposit (Fig. S3). No age estimate is available for Tephra 19 (UA 3074), although its stratigraphic position indicates it was deposited prior to the Holocene Hayes set H tephra (*ca.* 4000 a).

3.2. Tephra deposits originating from Iceland

Five deposits are identified as originating from Icelandic volcanic sources. Three deposits are of basaltic composition (NGRIP 1091.20 m GRIP 1245.58 m and NGRIP 1146.05 m), one shows an evolutionary trend from dacite to rhyolite (NGRIP 752.05 m) and one reveals a bimodal composition (NGRIP 753.90 m) with a dominant transitional basalt population and a smaller transitional trachyte population (Table 2, Figs. 3 and 6).

3.2.1. NGRIP 752.05 m: Hekla 4

The majority of shards extracted from the youngest deposit, NGRIP 752.05 m (4325 ± 8 a b1.95k), are of rhyolitic composition with highly evolved SiO_2 concentrations (74.74–76.22 wt%), total alkali values of ~6.64–8.26 wt% and FeO_t values ranging between 1.60 and 2.11 wt% (Figs. 3 and 6). Two glass shards from this deposit are dacitic, and one is basaltic, giving rise to the trends seen in Figs. 3 and 6. Hekla, one of Iceland's main silicic magmatic systems during the Holocene, is characterised by a distinct dacitic to rhyolitic evolutionary trends (e.g. Larsen and Thorarinsson, 1977; Sverrisdóttir, 2007). In particular, this type of compositional array is diagnostic of tephra products from the Hekla 4 and Hekla S eruptions that fall within *ca.* 500 years of the age of the NGRIP 752.05 m deposit (Fig. 6A and B). The most evolved component of NGRIP 752.05 m, however, shows a strong compositional affinity to Hekla 4 products based on CaO vs K_2O, and FeO_t and TiO_2 plots (Fig. 6) (Dugmore et al., 1995b; Wastegård et al., 2008; Meara et al., 2020). The dominant silicic component observed in NGRIP is also the most widely dispersed component found in distal settings throughout northern Europe (e.g. Dugmore, 1989; Dugmore et al., 1992; Dugmore et al., 1995b; Pilcher et al., 2005; Wulf et al., 2016). NGRIP 752.05 m is, therefore, correlated to the Hekla 4 Plinian eruption (Fig. 6).

3.2.2. NGRIP 753.90 m: a Katla tephra

NGRIP 753.90 m was deposited on the Greenland ice sheet 6–22 years before the Hekla 4 eruption (NGRIP 752.05 m) and is constrained in age to 4338 ± 8 a b1.95k. Twenty-seven glass shards form the dominant transitional basaltic composition, five shards comprise a trachydacite population and one outlier basaltic andesite shard is observed
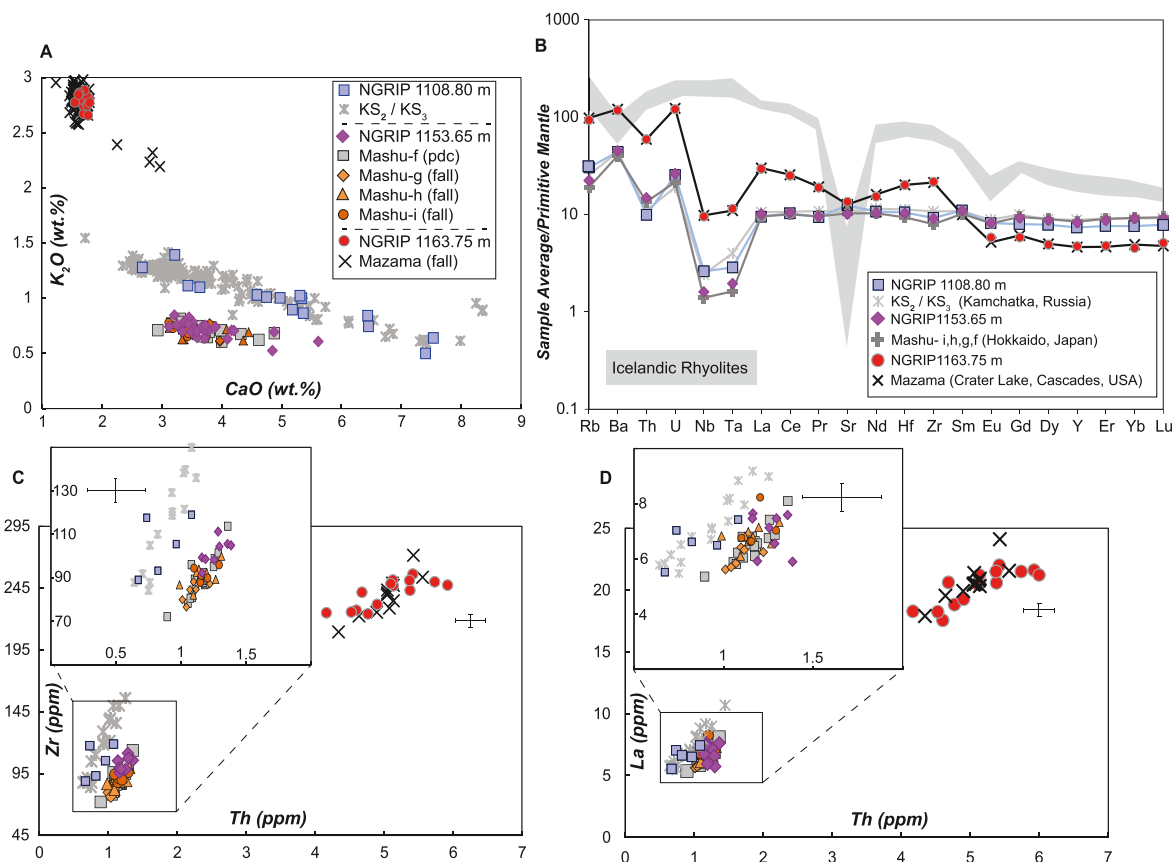
Fig. 4. Major and trace element analyses for NGRIP 1108.80 m, NGRIP 1153.65 m and NGRIP 1163.75 m. All major element data are normalised. **A.** CaO vs K_2O bivariate plot. **B.** Mantle-normalised trace element profile. **C.** Th vs Zr bivariate plot. **D.** Th vs La bivariate plot. Reference data for Mazama are from this study; Mashu-f (pdc: pyroclastic density current deposit) data are from the near-field sample presented in Albert et al. (2019) and Mashu i-g analyses are from this study; KS_2 and KS_3 data are from Portnyagin et al. (2020) and the Icelandic rhyolite envelope is based on Bourne et al. (2016).

(Fig. 3). The basaltic and trachydacite populations share affinity with typical mafic and silicic Katla products (Fig. 6) (Óladóttir et al., 2005, 2008). In particular, the trachydacite population, which is marked by SiO_2 concentrations of ~65 wt%, CaO values of ~3.6 wt% and K_2O values of ~2.7 wt% shows strong affinity to the silicic tephra layers derived from the Katla volcano, referred to as the SILK layers (Larsen et al., 2001a) (Fig. 6). A few trachydacitic shards of similar composition have also been identified mixed within a Hekla 4 cryptotephra deposit extracted from peat bogs at Glen West (GW173-175; Plunkett et al., 2004) and Claraghmore Bog in Northern Ireland (CLA-B6-B7; Watson et al., 2016) (Fig. 6). Both studies indicate a close stratigraphic association between Hekla 4 and a silicic Katla event. Making a correlation to a specific SILK layer, however, is not straight-forward.

At least 12 SILK deposits of Holocene age have been described by Larsen et al. (2001a) and dated by the soil accumulation rate method (Óladóttir et al., 2005). SILK-N2, dated to *ca.* 5000 a, is the closest in composition and age to NGRIP 753.90 m (Fig. 6B) and is found stratigraphically below the Hekla 4 deposit in soil sections to the east of the Katla volcano (Óladóttir et al., 2005, 2008). However, at least eight other ashfall deposits are observed between Hekla 4 and SILK-N2 in these proximal soil sections and given that the mean eruption frequency for Katla is thought to be four eruptions per century during prehistoric times, it is difficult to make an unequivocal correlation to the SILK-N2 layer (Óladóttir et al., 2005).

Frustratingly, the dominant basaltic component of NGRIP 753.90 m does not provide any further clues to aid a correlation to a SILK deposit. Six basaltic ashfall deposits from Katla (labelled HA-3 to HA-10 in Fig. 6D) have been analysed between the Hekla 4 and SILK-N2 deposits in a soil section at Atley to the east of Katla by Óladóttir et al. (2008).

Only mean values are available for comparison, with HA-4 showing the closest compositional match (Fig. 6D). Óladóttir et al. (2008) note that a few sparse silicic grains are found in some of these Katla basaltic deposits, but only one dacitic shard in HA-10 was identified within the series of basaltic deposits between Hekla 4 and SILK-N2 (Fig. 6A and B). Watson et al. (2016) also report one basaltic shard in the Hekla 4 deposit in Claraghmore Bog (CLA-B6-B7), but this is not a match for NGRIP 753.90 m (Fig. 6D).

Based on the evidence available to us, we are unable to correlate NGRIP 753.90 m to a specific event, but together with the evidence from Northern Ireland, we highlight that the Hekla 4 eruption was preceded by a closely timed SILK-like and basaltic Katla eruption.

3.2.3. Icelandic basaltic eruptions: NGRIP 1146.05 m, GRIP 1245.58 m and NGRIP 1091.20 m

Major element results for the three basaltic deposits reveal scattered compositional populations (Fig. 6E). Only six shards were analysed in NGRIP 1091.20 m, which is dated to 6943 ± 23 a b1.95k. Three shards from NGRIP 1091.20 m exhibit Katla signatures (Mean FeO_t value of 13.96 wt% and TiO_2 values of 3.91 wt%) and two shards show closer affinity with Hekla-Vatnafjöll with TiO_2 values < 3.5 wt% (Fig. 6E). GRIP 1245.58 m is constrained in age to 7353 ± 32 a b1.95k and is the most scattered of these three basaltic deposits (Fig. 6E), showing affinity to Grimsvötn, Hekla/Vatnafjöll and Katla envelopes (Fig. 6E). Dated to 7410 ± 32 a b1.95k, NGRIP 1146.05 m is slightly older than GRIP 1245.58 m, and also shows prominent compositional ranges in FeO_t, MgO and CaO but appears to have two distinct populations. The dominant population (13 shards) has a MgO range of 7.47–7.92 wt% and mean values of K_2O, TiO_2 and FeO_t that are <0.2 wt%, 1.45 wt% and
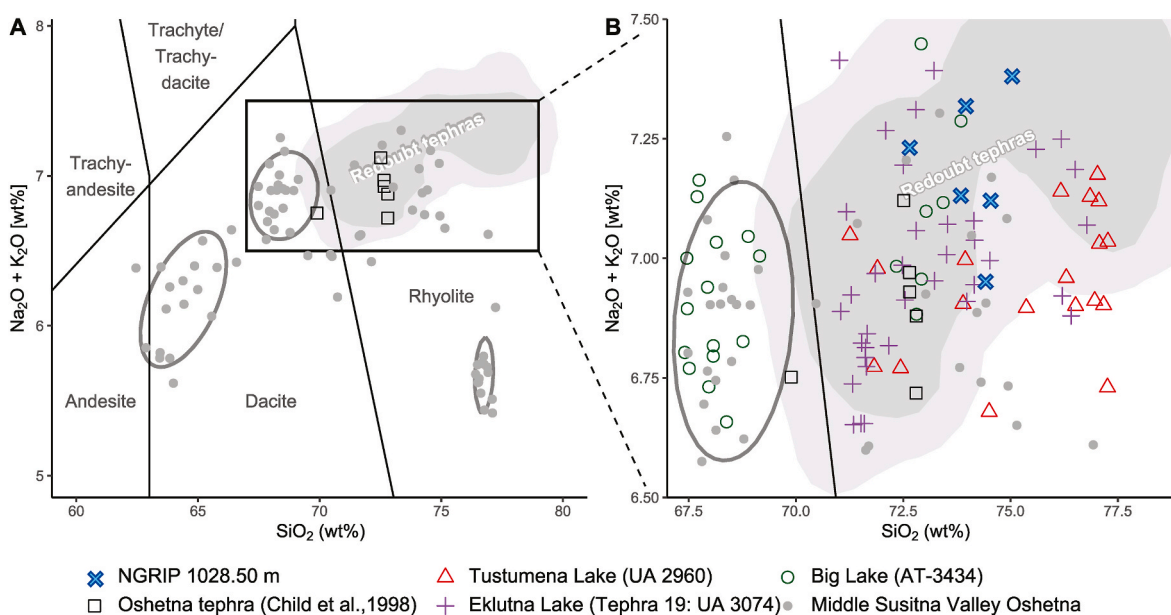
Fig. 5. Total alkali-silica diagram for NGRIP 1028.50 m. The compositional field of known Redoubt tephras is derived from the training data outlined in Bolton et al. (2020) and supplemented with Redoubt tephras identified therein. Shaded polygons indicate regions of 68% and 90% highest density and potentially related Redoubt/"Oshetna" tephras. **A** shows "Oshetna" shards from Child et al. (1998), whose compositions overlap in part with the Redoubt field, while three other populations found in the Middle Susitna Valley "Oshetna" samples (AT-3188, AT-3183, AT-3193, AT-3196) from Mulliken (2016) and Bigelow et al. (2019) are indicated by grey ellipses. **B** shows the area enclosed by the rectangle in A and includes the single-shard analyses from NGRIP 1028.50 m along with tephras from Tustumena Lake (UA 2960), Eklutna Lake (UA 3074) and Big Lake (AT-3434). Compositional classifications are based on Le Maitre (1989). Full details of the data-set included in this Figure are available in Supplementary Information 2.

11.06 wt% respectively (Supplementary Information 1). This composition is typical of the Veidivötn-Bárdarbunga system (Óladóttir et al., 2011b) (Fig. 6E). A further seven shards extracted from NGRIP 1146.05 m have a more scattered composition with higher K_2O values ranging between 0.32 and 0.66 wt%, TiO_2 values of 2.42–3.30 wt%, a higher FeO_t average of 13.69 wt% and a lower MgO average of 5.50 wt%. These characteristics show affinity with Grímsvötn (Óladóttir et al., 2011b). FeO_t/TiO_2 is a further discriminant that suggests the two populations of NGRIP 1146.05 m originated from different sources (i.e. 7.6 vs 4.8 is indicative of Veidivötn-Bárdarbunga and Grimsvötn sources, respectively) (Óladóttir et al., 2008, 2011b).

Although Icelandic sources are suggested for these three basaltic deposits, pinpointing a specific correlative event is more challenging. Several Middle Holocene ashfall deposits originating from Katla, Veidivötn-Bardarbunga and Grimsvötn have been identified in soil, lake and offshore marine records in Iceland (Óladóttir et al., 2005, 2008, 2011a, 2011b; Gudmundsdóttir et al., 2012, 2016, 2018). Many of these have very similar compositional signatures, and thus, pinpointing which ones are present in the ice is problematic. We note, however, the compositional similarities to tephras identified in marine core MD99-2275 from the North Atlantic shelf (Gudmundsdóttir et al., 2012) and a sediment record from Lake Lögurinn in eastern Iceland (Gudmundsdóttir et al., 2016) (Fig. 6E).

We recommend that the search for firm correlations in other sequences should focus on searching for an ashfall couplet close in age that exhibit Veidivötn-Bardarbunga and Grimsvötn signatures (i.e. NGRIP 1146.05 m and GRIP 1245.58 m). Trace element analyses may also aid in the correlation to specific basaltic events.

4. Discussion

The suite of Holocene ashfall discoveries presented here highlights the pivotal position of the Greenland ice cores in repeatedly capturing ashfall deposition from the convergence of several far-travelled ash clouds (Fig. 7). Our findings are significant for three main reasons. First,

the value of these isochrons for correlation purposes is greatly enhanced. The discovery of tephras from five different volcanic source regions (Alaska, Cascades, Iceland, Japan and Kamchatka) widens the geographical extent of ash dispersal and significantly expands the possibilities of using cryptotephras to precisely correlate palaeorecords across the northern hemisphere during the Holocene. One particular gem is the Mashu discovery. Ash fallout from the Mashu i-f caldera-forming eruption was thought to have been geographically limited, despite being classified as a VEI 6 eruption (Crosweller et al., 2012) with a bulk tephra volume estimate of 18.6 km^3 (Kishimoto et al., 2009). No fallout has been previously detected beyond the island of Hokkaido, Rebun Island in the Sea of Japan (Chen et al., 2019), and the southern Kurile Islands (Razzhigaeva et al., 2016). Its discovery in Greenland, therefore, significantly extends the geographical extent of known ash fallout and enhances the value of this chemically distinctive low-K deposit as a widespread isochron. Furthermore, tracing Hekla 4 in the Greenland ice-core records now allows a whole suite of lake and varve records in Europe (e.g. Diss Mere, Walsh et al., 2023), which preserves a Hekla 4 deposit, to be precisely correlated or synchronised to NGRIP. This isochron is ideally placed to investigate the climatic and environmental changes associated with the *ca.* 4200 a event in Europe (e.g. Walsh et al., 2023). A further correlation step may also be facilitated by using the ice-core record as a linchpin whereby the European records, that preserve the Hekla 4 isochron, could be synchronised to North American or Kamchatkan palaeoarchives courtesy of the position of the Mazama and/or the KS_2 deposits in the NGRIP record (Fig. 7).

Second, these discoveries have a significant role to play in building a global record of volcanism and highlight the role of polar ice-core records, located some distance from volcanic sources, in archiving prehistoric ashfall events that may be lost from near-field records, often subject to the destructive forces of subsequent eruptions and erosional processes. Here, we show that major and trace element geochemical analyses of volcanic glass shard analyses and annually resolved age constraints for each ashfall event allows the source to be pinpointed. Many sulphate peaks observed in glaciochemical records are essentially
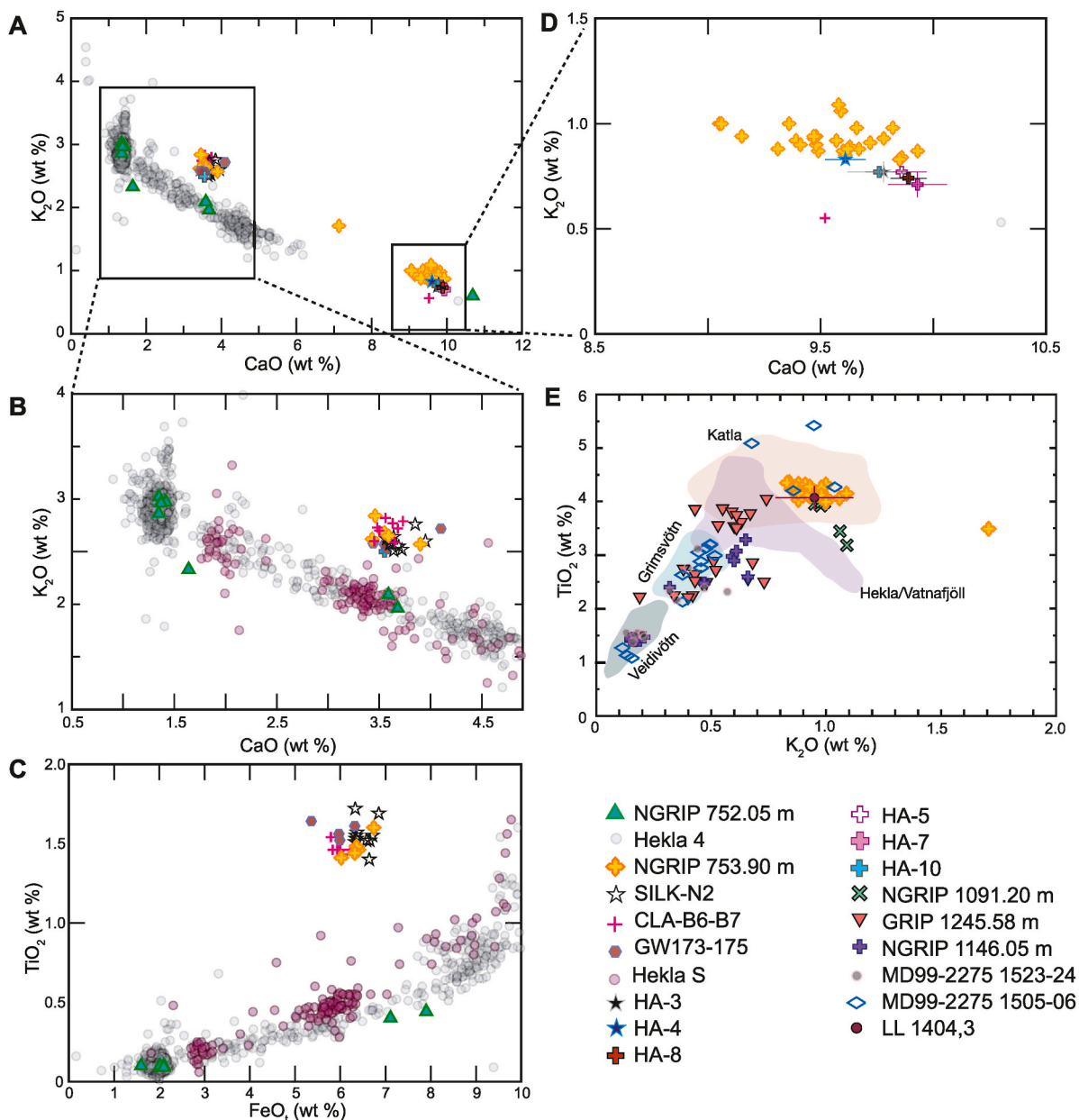
Fig. 6. Major element data for NGRIP and GRIP tephras originating from Iceland. All data are normalised and total Fe is reported as FeO$_t$. **A-D.** NGRIP 752.05 m is plotted relative to Hekla 4 and Hekla S data; NGRIP 753.90 m is plotted relative to Katla silicic and basaltic tephras. Reference data for Hekla 4 and Hekla S were obtained from Tephrabase (www.tephrabase.org) and include the following data-sets (Boygle, 1994, 1998, 2004; Dugmore, 1989; Dugmore et al., 1992, 1995b; Dugmore and Newton, 1997; Gudmundsdóttir et al., 2011a; Hang et al., 2006; Meara et al., 2020; Óladóttir et al., 2011a; Pilcher et al., 1995, 1996, 2005; Pilcher and Hall, 1996; Roland et al., 2014; Swindles, 2006; van den Bogaard and Schmincke, 2002; Vorren et al., 2007; Wastegård, 2005; Wastegård et al., 2001; Watson et al., 2016; Wulf et al., 2016; Zillén et al., 2002). SILK-N2 data are from Larsen et al. (2001b), Claraghmore Bog CLA-B6-B7 data are from Watson et al. (2016), Glen West GW 173–175 data are from Plunkett et al. (2004). **D.** HA-3, -4, -5, -7, -8 and -10 are from Óladóttir et al. (2008). **E.** NGRIP 1091.20 m, GRIP 1245.58 m and NGRIP 1146.05 m are plotted relative to source envelopes based on geochemical data reported in Jakobsson (1979), Boygle (1994), Hunt et al. (1995), Dugmore and Newton (1997), Haflidason et al. (2000), Davies et al. (2001), Wastegård et al. (2001), Larsen et al. (2002), Mortensen et al. (2005) and Óladóttir et al. (2008). MD99-2275 1523–24 cm and 1505–06 cm are from Gudmundsdóttir et al. (2012), LL1404,3 data are from Gudmundsdóttir et al. (2016). Where errors bars are shown these are 1 sigma standard deviation.

unassigned or unidentified in terms of volcanic source, without constraints from volcanic glass shards found in association with a sulphate spike. Thus, the approach we adopt here also enhances the value of the volcanic forcing indices derived largely from ice-core sulphate records (e.g. Sigl et al., 2015; Sigl et al., 2022).

A third significance of these discoveries is the generation of new and more precise age estimates for each event, derived directly from the ice-core chronology (Fig. 8). In particular, Hekla 4 is found in palaeo-records, including varve records, throughout northern Europe (Fig. 7)

and the ice-core derived age of 4325 ± 8 a b1.95k will be a hugely valuable chronological tie-point in developing age-depth models where this isochron can be traced. Although the ice-core age falls within the previously published age ranges derived from radiocarbon dating of Irish peats (Pilcher et al., 1996) and varve records from Sweden (Zillén et al., 2002) and Germany (Dörfler et al., 2012), this new age constrains the timing of the Hekla 4 more precisely (Fig. 8). The ice-core age diverges from the radiocarbon estimate derived from Scottish peats (Dugmore et al., 1995a) and the most recently reported age from the
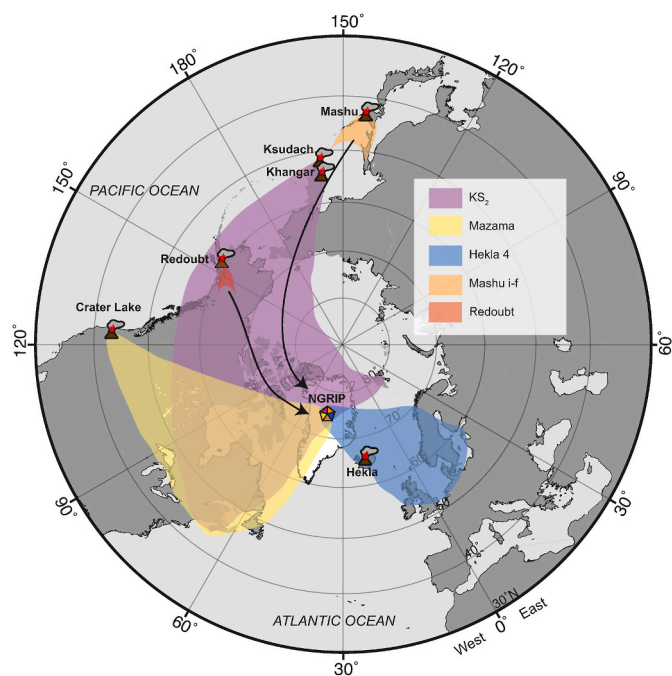
Fig. 7. Schematic illustration of the geographical extent of the Mazama, KS$_2$ and Hekla 4 tephra fallout constrained by the NGRIP discoveries (pentagon) and previously published findings. The distribution of Mazama includes the distal findings within Nordan's Pond Bog, Newfoundland (Pyne-O'Donnell et al., 2012), Keweenaw Bay and Isle Royale, Lake Superior (Spano et al., 2017), Bloomingdale Bog NY State, Thin Ice Pond, Sidney Bog (Jensen et al., 2021) and GISP2 (Zdanowicz et al., 1999). KS$_2$ distribution includes Lake Hajeren, Svalbard (van der Bilt et al., 2017) and Thin Ice Pond, Nova Scotia (Jensen et al., 2021). The Hekla 4 envelope is modified after Wulf et al. (2016), Cooper et al. (2019) and Walsh et al. (2023). Black arrows show possible transport routes for Mashu i-f and the Redoubt tephra to Greenland. The location of the Khangar volcano, which also generated tephra that was deposited in Greenland ice in the Early Holocene is also shown (Cook et al., 2018).

Diss Mere varve record (Walsh et al., 2023). The discrepancy with the Diss Mere record may result from uncertainties in varve preservation and the Bayesian modelling approach used to integrate radiocarbon ages with the floating varve chronology (Martin-Puertas et al., 2021). Perhaps the new ice-core age may prove valuable as a new fix-point for the Diss Mere record. Furthermore, a more precise age estimate also holds considerable potential for testing radiocarbon reservoir ages in areas where Hekla 4 preservation extends into the marine environment (e.g. Gudmundsdóttir et al., 2012).

An ice-core age for KS$_2$ of 7089 ± 26 a b1.95k also considerably improves the existing broad radiocarbon age estimates which range from 7400 to 6600 cal a BP, if all uncertainties are considered (Fig. 8). Radiocarbon age estimates from proximal material constrain the KS$_2$ eruption to between 6877 and 6693 cal a BP (Ponomareva et al., 2017). However, AMS radiocarbon age determinations, derived from crypto-tephra deposits preserved in lake sediments on the Kamchatkan peninsula and as far afield as Nova Scotia, have suggested that the age range derived from proximal deposits is too young. These cryptotephra studies report age ranges of 7350–7180 cal a BP and 7300–7160 cal a BP (Plunkett et al., 2015), 7204 cal a BP (Pendea et al., 2017) and 7185–6970 cal a BP within the Thin Ice Pond record from Nova Scotia (Jensen et al., 2021). The ice-core age resolves the divergent age ranges for this eruption and provides a more precise age constraint for palae-orecords that contain this widespread marker horizon.

Chen et al. (2022) recently presented a Bayesian analysis of all ^{14}C datasets derived from near-field deposits of Mashu f-j deposits and outline an eruption age at 7670–7395 cal a BP (95.4%). The ice-core age falls within this range and significantly reduces the error estimates
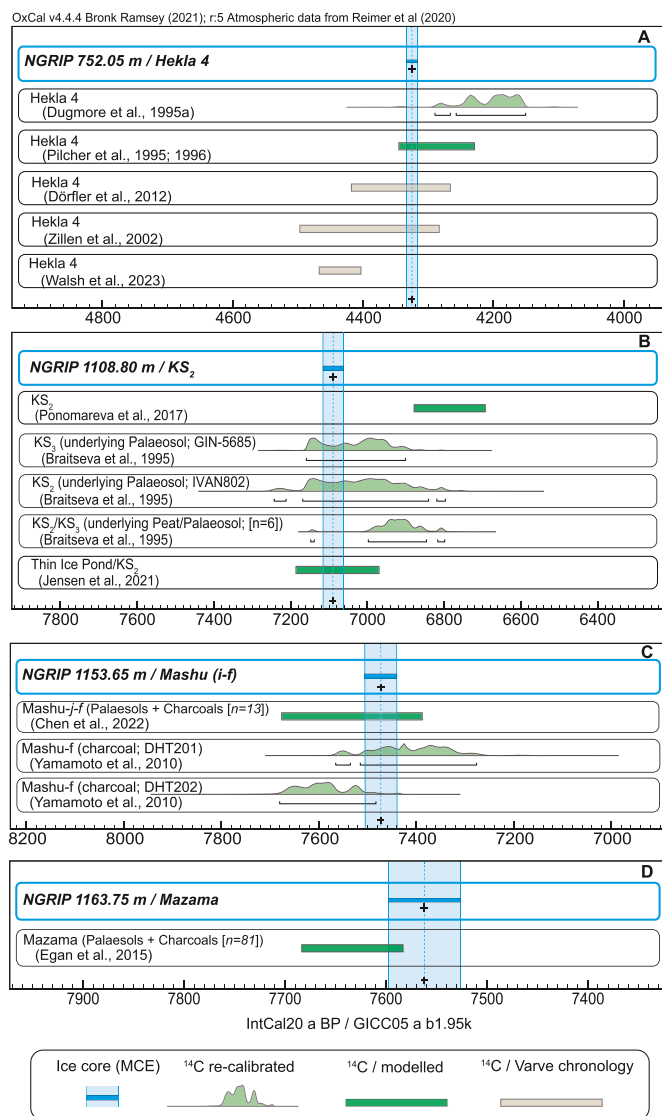

Fig. 8. Summary of the new tephra ages for Hekla 4 (A), KS$_2$ (B), Mashu i-f (C) and Mazama (D) based on their position in the NGRIP ice-core record. Ice-core ages are plotted as GICC05 a b1.95k (see Table 2) to facilitate comparisons to previously published age estimates that are derived from radiocarbon age estimates and varve records. Radiocarbon age estimates from the original studies are re-calibrated here using IntCal20 (Reimer et al., 2020) (labelled as ^{14}C/re-calibrated). However, if the original study employed a modelling approach (e.g. wiggle matching or Bayesian analysis), then the derived calendar age, as reported in the original study, is presented (labelled as ^{14}C/modelled). All ages are shown with 2 sigma uncertainties. The Maximum Counting Error (MCE) for the ice-core ages is typically considered to be equivalent to 2 sigma uncertainties. GIN, IVAN and DHT are radiocarbon laboratory codes reported in the indicated references.

associated with this event (7473 ± 33 a b1.95k). The Mazama ice-core age estimate of 7562 ± 35 a b1.95k partially overlaps with the previously reported range of 7682–7584 cal a BP (95.4%) derived from Bayesian modelling of extensive radiocarbon data from charcoals and palaeosols associated with the Mazama eruption (Egan et al., 2015). The Greenland ice-core age is consistent with the age of 5622 BCE or 7572 cal a BP reported in the Holocene volcanic forcing data-set presented by Sigl et al. (2022). An ice-core age estimate for the Redoubt tephra (NGRIP 1028.50 m) also offers a new age constraint in developing age models for Alaskan palaeolake records, that was hitherto not available (de Fontaine et al., 2007) (see Fig. S3, Supplementary Information 3).

Exploiting the volcanic glass record archived within the polar ice-

cores depends entirely on the culmination of several conditions i.e. an ash transport trajectory towards the pole, deposition and preservation at the ice-core drill site, and our ability to detect and manipulate microscopic glass shards. In many instances, glass shards from ashfall events far removed from the poles will prove elusive or be difficult to geochemically fingerprint. For instance, the large sulphate spike at 7240 $\pm$ 27 b2k is not accompanied by any glass shards in NGRIP, meaning that the source of this high-sulphate loading event remains unidentified (Fig. 1), but may well relate to one of our initial target eruptions outlined in Table 1. For highly valuable and sought-after ashfall events, we recommend searching in more than one ice-core, to improve the chances of discovering sufficient glass shards e.g. Gabriel et al. (2024). Furthermore, where glass shards are present, major element data, in some instances, may not be sufficient to support a correlation. Where possible we demonstrate the value of trace element analyses and recommend their use as an additional characterisation tool, especially where ultra-distal correlations are proposed.

We also recommend that cryptotephra sampling strategies go beyond solely constraining searches associated with large glaciochemical signals. Typically, large sulphate, electrical conductivity measurements or dielectric signals (DEP) underpin many targeted sampling campaigns to identify the presence of volcanic glass shards, especially in association with eruptions that are thought to have climatic and/or societal impacts. Plunkett et al. (2023) also outline the value of focussing on continuous microparticle records from ice-cores for tephra investigations as well as exploring the relative timing of ash and sulphate deposition. Whilst these targeted sampling efforts can reap rewards for assigning sources to unidentified large sulphur-loading events (e.g. McConnell et al., 2020), such focused work also increases the possibility that cryptotephra deposits, which offer considerable value for correlation and age-modelling constraints, may be overlooked. For instance, tephra from the Hekla 4, KS_2 and Mashu i-f caldera-forming eruptions may have been missed if sampling efforts focused solely on large glaciochemical peaks (Fig. 1). This observation aligns with many studies of tephras preserved within pre-Holocene ice (e.g. Bourne et al., 2015; Cook et al., 2022). Our targeted searches for the Hekla 3 and Glen Garry tephras in this study may prove more fruitful if our sampling intervals are extended. Thus, depending on the intended use of cryptotephra deposits in the ice, if we are to fill gaps in our knowledge of the global volcanic record (Self and Gertisser, 2015), then sampling ice-cores over continuous time intervals is essential.

5. Summary and conclusions

- Nine Middle Holocene tephra deposits are identified within the NGRIP and GRIP ice-cores underscoring the value of polar ice-cores in reconstructing a global volcanic record. Tephras originating from five different volcanic source regions (Alaska, Cascades, Iceland, Japan and Kamchatka) highlight the convergence of ancient ash clouds over the Greenland ice-sheet and the pivotal role of these distal records in filling gaps in the global volcanic record.
- Three deposits originating from caldera-forming eruptions at circum-Pacific arc volcanoes are identified within a 500-year window: Crater Lake (Mazama), KS_2 from Ksudach and Mashu i-f.
- Hekla 4, a widespread marker horizon in lake (including varved records) and marine sediment records in Europe, is also identified along with three Icelandic basaltic deposits and one bimodal deposit.
- Precise ice-core age estimates are outlined for each tephra deposit, significantly enhancing their value as isochrons and fix-points in palaeoarchives where the same tephra can be traced.

Data availability statement

All data in this article are avilable in the supplementary files. These data are also available on the Zenodo data repository 10.5281/zenodo.11186116.

CRediT authorship contribution statement

Siwan M. Davies and **Paul G. Albert:** Conceptualisation, Investigation, Data curation/Formal analysis, Writing – original draft, Writing – review and editing (+**SMD**: Funding acquisition). **Anna J. Bourne:** Data curation/Formal analysis, Writing – review and editing. **Sara Owen:** Data curation/Formal analysis, Writing – review and editing. **Anders Svensson:** Data curation/Formal analysis, Visualisation, Writing – review and editing. **Matthew S. M. Bolton:** Data curation/Formal analysis, Writing – review and editing. **Eliza Cook:** Data curation, Writing – review and editing. **Britta J. L. Jensen:** Data curation/Formal analysis, Writing – review and editing. **Gwydion Jones:** Data curation, Visualisation, Writing – review and editing. **Vera V. Ponomareva:** Data curation/Formal analysis, Writing – review and editing. **Takehiko Suzuki:** Data curation, Writing – review and editing.

Declaration of competing interest

The authors declare that they have no known competing financial interests or personal relationships that could have appeared to influence the work reported in this paper.

Data availability

All data used in this article are available in the supplementary files. These data are also available on the Zenodo data repository **10.5281/zenodo.11186116.**

Acknowledgements

Appendix A. Supplementary data

Supplementary data to this article can be found online at https://doi.

org/10.1016/j.quascirev.2024.108707.

References

Abbott, P.M., Davies, S.M., Steffensen, J.P., Pearce, N.J.G., Bigler, M., Johnsen, S.J., Seierstad, I.K., Svensson, A., Wastegård, S., 2012. A detailed framework of Marine Isotope Stages 4 and 5 volcanic events recorded in two Greenland ice-cores. Quat. Sci. Rev. 36, 59–77.

Adolphi, F., Muscheler, R., 2016. Synchronizing the Greenland ice core and radiocarbon timescales over the Holocene – Bayesian wiggle-matching of cosmogenic radionuclide records. Clim. Past 12, 15–30.

Albert, P.G., Smith, V.C., Suzuki, T., McLean, D., Tomlinson, E.L., Miyabuchi, Y., Kitaba, I., Mark, D.F., Moriwaki, H., Nakagawa, T., 2019. Geochemical characterisation of the Late Quaternary widespread Japanese tephrostratigraphic markers and correlations to the Lake Suigetsu sedimentary archive (SG06 core). Quat. Geochronol. 52, 103–131.

Andersen, K.K., Svensson, A., Johnsen, S.J., Rasmussen, S.O., Bigler, M., Rothlisberger, R., Ruth, U., Siggaard-Andersen, M.-L., Steffensen, J.P., Dahl-Jensen, D., Vinther, B.M., Clausen, H.B., 2006. The Greenland Ice Core Chronology 2005, 15-42 ka. Part 1: constructing the time scale. Quat. Sci. Rev. 25, 3246–3257.

Bacon, C.R., 1983. Eruptive history of Mount Mazama and Crater Lake Caldera, Cascade Range, U.S.A. J. Volcan. Geotherm. Res. 18, 57–115.

Barber, K., Langdon, P., Blundell, A., 2008. Dating the Glen Garry tephra: a widespread late-Holocene marker horizon in the peatlands of northern Britain. Holocene 18, 31–43.

Bigelow, N.H., Reuther, J.D., Wallace, K.L., Saulnier-Talbot, É., Mulliken, K., Wooler, M. J., 2019. Late-Glacial Paleoecology of the Middle Susitna Valley, Alaska: Environmental Context for Human Dispersal. Front. Earth Sci. 7, 43.

Bolton, M.S.M., Jensen, B.J.L., Wallace, K., Praet, N., Fortin, D., Kaufman, D., De Batist, M., 2020. Machine learning classifiers for attributing tephra to source volcanoes: an evaluation of methods for Alaska tephras. J. Quat. Sci. 35, 81–92.

Bourne, A.J., Abbott, P.M., Albert, P.G., Cook, E., Pearce, N.J.G., Ponomareva, V., Svensson, A., Davies, S.M., 2016. Underestimated risks of recurrent long-range ash dispersal from northern Pacific Arc volcanoes. Sci Rep-Uk 6, 29837.

Bourne, A.J., Cook, E., Abbott, P.M., Seierstad, I.K., Steffensen, J.P., Svensson, A., Fischer, H., Schüpbach, S., Davies, S.M., 2015. A tephra lattice for Greenland and a reconstruction of volcanic events spanning 25–45 ka b2k. Quat. Sci. Rev. 118, 122–141.

Boygle, J., 1998. A little goes a long way: discovery of a new mid-Holocene tephra in Sweden. Boreas 27, 195–199.

Boygle, J., 2004. Towards a Holocene tephrochronology for Sweden: geochemistry and correlation with the North Atlantic tephra stratigraphy. J. Quat. Sci. 19, 103–109.

Boygle, J.E., 1994. Tephra in Lake Sediments: an Unambiguous Geochronological Marker? Unpublished PhD Thesis. University of Edinburgh, Edinburgh.

Braitseva, O.A., Melekestsev, I.V., Ponomareva, V.V., Sulerzhitsky, L.D., 1995. Ages of calderas, large explosive craters and active volcanoes in the Kuril-Kamchatka region, Russia. Bull. Volcanol. 57, 383–402.

Braitseva, O.A., Ponomareva, V.V., Sulerzhitsky, L.D., Melekestsev, I.V., Bailey, J., 1997. Holocene Key-Marker Tephra Layers in Kamchatka, Russia. Quat. Res. 47, 125–139.

Bronk Ramsey, C., 2008. Deposition models for chronological records. Quat. Sci. Rev. 27, 42–60.

Buckland, H.M., Cashman, K.V., Engwell, S.L., Rust, A.C., 2020. Sources of uncertainty in the Mazama isopachs and the implications for interpreting distal tephra deposits from large magnitude eruptions. Bull. Volcanol. 82, 23.

Chen, X.Y., Blockley, S.P.E., Staff, R.A., Xu, Y.G., Menzies, M.A., 2022. Improved age estimates for Holocene Ko-g and Ma-f-j tephras in northern Japan using Bayesian statistical modelling. Quat. Geochronol. 67, 101229.

Chen, X.Y., McLean, D., Blockley, S.P.E., Tarasov, P.E., Xu, Y.G., Menzies, M.A., 2019. Developing a Holocene tephrostratigraphy for northern Japan using the sedimentary record from Lake Kushu, Rebun Island. Quat. Sci. Rev. 215, 272–292.

Child, J.K., Begét, J.E., Werner, A., 1998. Three Holocene Tephras Identified in Lacustrine Sediment Cores from the Wonder Lake Area, Denali National Park and Preserve, Alaska. U.S.A. Arctic and Alpine Research 30, 89–95.

Cook, E., Abbott, P.M., Pearce, N.J.G., Mojtabavi, S., Svensson, A., Bourne, A.J., Rasmussen, S.O., Seierstad, I.K., Vinther, B.M., Harrison, J., Street, E., Steffensen, J. P., Wilhelms, F., Davies, S.M., 2022. Volcanism and the Greenland ice cores: A new tephrochronological framework for the last glacial-interglacial transition (LGIT) based on cryptotephra deposits in three ice cores. Quat. Sci. Rev. 292, 107596.

Cook, E., Portnyagin, M., Ponomareva, V., Bazanova, L., Svensson, A., Garbe-Schönberg, D., 2018. First identification of cryptotephra from the Kamchatka Peninsula in a Greenland ice core: Implications of a widespread marker deposit that links Greenland to the Pacific northwest. Quat. Sci. Rev. 181, 200–206.

Cooper, C.L., Swindles, G.T., Watson, E.J., Savov, I.P., Gałka, M., Gallego-Sala, A., Borken, W., 2019. Evaluating tephrochronology in the permafrost peatlands of northern Sweden. Quat. Geochronol 50, 16–28.

Coulter, S.E., Pilcher, J.R., Plunkett, G., Baillie, M., Hall, V.A., Steffensen, J.P., Vinther, B.M., Clausen, H.B., Johnsen, S.J., 2012. Holocene tephras highlight complexity of volcanic signals in Greenland ice cores. J. Geophys. Res. Atmos. 117.

Crosweller, H.S., Arora, B., Brown, S.K., Cottrell, E., Deligne, N.I., Guerrero, N.O., Hobbs, L., Kiyosugi, K., Loughlin, S.C., Lowndes, J., Nayembil, M., Siebert, L., Sparks, R.S.J., Takarada, S., Venzke, E., 2012. Global database on large magnitude explosive volcanic eruptions (LaMEVE). J. Appl. Volcanol. 1, 4.

Davies, S.M., Abbott, P.M., Meara, R.H., Pearce, N.J.G., Austin, W.E.N., Chapman, M.R., Svensson, A., Bigler, M., Rasmussen, T.L., Rasmussen, S.O., Farmer, E.J., 2014. A North Atlantic tephrostratigraphical framework for 130–60 ka b2k: new tephra discoveries, marine-based correlations, and future challenges. Quat. Sci. Rev. 106, 101–121.

Davies, S.M., Turney, C.S.M., Lowe, J.J., 2001. Identification and significance of a visible, basalt-rich Vedde Ash layer in a Late-glacial sequence on the Isle of Skye, Inner Hebrides, Scotland. J. Quat. Sci. 16, 99–104.

Davies, S.M., Wastegård, S., Abbott, P.M., Barbante, C., Bigler, M., Johnsen, S.J., Rasmussen, T.L., Steffensen, J.P., Svensson, A., 2010. Tracing volcanic events in the NGRIP ice-core and synchronising North Atlantic marine records during the last glacial period. Earth Planet Sci. Lett. 294, 69–79.

de Fontaine, C.S., Kaufman, D.S., Scott Anderson, R., Werner, A., Waythomas, C.F., Brown, T.A., 2007. Late Quaternary distal tephra-fall deposits in lacustrine sediments, Kenai Peninsula, Alaska. Quat. Res. 68, 64–78.

De Silva, S.L., Zielinski, G.A., 1998. Global influence of the AD1600 eruption of Huaynaputina, Peru. Nature 393, 455–458.

Dixon, E.J., 1985. Cultural chronology of central interior Alaska. Arctic Anthropol. 22, 47–66.

Dixon, E.J., Smith, G.S., 1990. A regional application of tephrochronology in Alaska. In: Lasca, N.P., Donahue, J. (Eds.), Archaeological Geology of North America. Geological Society of America, Boulder, pp. 383–398.

Dörfler, W., Feeser, I., van den Bogaard, C., Dreibrodt, S., Erlenkeuser, H., Kleinmann, A., Merkt, J., Wiethold, J., 2012. A high-quality annually laminated sequence from Lake Belau, Northern Germany: Revised chronology and its implications for palynological and tephrochronological studies. Holocene 12, 1413–1426.

Dräger, N., Theuerkauf, M., Szeroczyńska, K., Wulf, S., Tjallingii, R., Plessen, B., Kienel, U., Brauer, A., 2016. Varve microfacies and varve preservation record of climate change and human impact for the last 6000 years at Lake Tiefer See (NE Germany). Holocene 27, 450–464.

Dugmore, A.J., 1989. Icelandic volcanic ash in Scotland. Scot. Geogr. Mag. 105, 168–172.

Dugmore, A.J., Cook, G.T., Shore, J.S., Newton, A.J., Edwards, K.J., Larsen, G., 1995a. Radiocarbon dating tephra layers in Britain and Iceland. Radiocarbon 37, 379–388.

Dugmore, A.J., Larsen, G., Newton, A.J., 1995b. Seven tephra isochrones in Scotland. Holocene 5, 257–266.

Dugmore, A.J., Newton, A.J., 1997. Holocene tephra layers in the Faroe Islands. Fróðskaparrit 46, 191–204.

Dugmore, A.J., Newton, A.J., Sugden, D.E., Larsen, G., 1992. Geochemical stability of fine grained silicic Holocene tephra in Iceland and Scotland. J. Quat. Sci. 7, 173–183.

Egan, J., Staff, R., Blackford, J., 2015. A high-precision age estimate of the Holocene Plinian eruption of Mount Mazama, Oregon, USA. Holocene 25, 1054–1067.

Gabriel, I., Plunkett, G., Abbott, P.M., Behrens, M., Burke, A., Chellman, N., Cook, E., Fleitmann, D., Hörhold, M., Hutchison, W., McConnell, J.R., Óladóttir, B.A., Preiser-Kapeller, J., Sliwinski, J.T., Sugden, P., Twarloh, B., Sigl, M., 2024. Decadal-to-centennial increases of volcanic aerosols from Iceland challenge the concept of a Medieval Quiet Period. Commun. Earth Environ. 5, 194.

Global Volcanism Program, Smithsonian Institution, 2023. Hekla in Database Volcanoes of the World (v.5.1.5; 15 Dec 2023), Distributed by Smithsonian Institution, Compiled by Venzke. E. https://volcano.si.edu/.

Grönvold, K., Oskarsson, N., Johnsen, S.J., Clausen, H.B., Hammer, C.U., Bond, G., Bard, E., 1995. Ash layers from Iceland in the GRIP ice core correlated with oceanic and land sediments. Earth Planet Sci. Lett. 135, 149–155.

Gudmundsdóttir, E.R., Eiríksson, J., Larsen, G., 2011a. Identification and definition of primary and reworked tephra in Late Glacial and Holocene marine shelf sediments off North Iceland. J. Quat. Sci. 26, 589–602.

Gudmundsdóttir, E.R., Larsen, G., Björck, S., Ingólfsson, Ó., Striberger, J., 2016. A new high-resolution Holocene tephra stratigraphy in eastern Iceland: Improving the Icelandic and North Atlantic tephrochronology. Quat. Sci. Rev. 150, 234–249.

Gudmundsdóttir, E.R., Larsen, G., Eiríksson, J., 2011b. Two new Icelandic tephra markers: The Hekla Ö tephra layer, 6060 cal. yr BP, and Hekla DH tephra layer, ~ 6650 cal. yr BP. Land-sea correlation of mid-Holocene tephra markers. Holocene 21, 629–639.

Gudmundsdóttir, E.R., Larsen, G., Eiríksson, J., 2012. Tephra stratigraphy on the North Icelandic shelf: extending tephrochronology into marine sediments off North Iceland. Boreas 41, 719–734.

Gudmundsdóttir, E.R., Schomacker, A., Brynjólfsson, S., Ingólfsson, Ó., Larsen, N.K., 2018. Holocene tephrostratigraphy in Vestfirðir, NW Iceland. J. Quat. Sci. 33, 827–839.

Haflidason, H., Eiríksson, J., van Kreveld, S., 2000. The tephrochronology of Iceland and the North Atlantic region during the Middle and Late Quaternary: a review. J. Quat. Sci. 15, 3–22.

Hang, T., Wastegård, S., Veski, S., Heinsalu, A., 2006. First discovery of cryptotephra in Holocene peat deposits of Estonia, eastern Baltic. Boreas 35, 644–649.

Hasegawa, T., Nakagawa, M., Kishimoto, H., 2012. The eruption history and silicic magma systems of caldera-forming eruptions in eastern Hokkaido, Japan. J. Mineral. Petrol. Sci. 107, 39–43.

Hayward, C., 2012. High spatial resolution electron probe microanalysis of tephras and melt inclusions without beam-induced chemical modification. Holocene 22, 119–125.

Hunt, J.B., Fannin, N.G.T., Hill, P.G., Peacock, J.D., 1995. The Tephrochronology and Radiocarbon Dating of North Atlantic, Late-Quaternary Sediments: an Example from the St. Kilda Basin, vol. 90. Geological Society, London, Special Publications, pp. 227–248.

Jakobsson, S.P., 1979. Petrology of recent basalts of the Eastern Volcanic Zone, Iceland. Acta Nat. Isl. 26, 1–103.

Jakobsson, S.P., Jónasson, K., Sigurdsson, I.A., 2008. The three igneous rock suites of Iceland. Jokull 58, 117–138.

Jensen, B.J.L., Davies, L.J., Nolan, C., Pyne-O'Donnell, S., Monteath, A.J., Ponomareva, V., Portnyagin, M., Booth, R., Bursik, M., Cook, E., Plunkett, G., Vallance, J.W., Luo, Y., Cwynar, L.C., Hughes, P., Pearson, D.G., 2021. A latest Pleistocene and Holocene composite tephrostratigraphic framework for northeastern North America. Quat. Sci. Rev. 272, 107242.

Jensen, B.J.L., Pyne-O'Donnell, S., Plunkett, G., Froese, D.G., Hughes, P.D.M., Sigl, M., McConnell, J.R., Amesbury, M.J., Blackwell, P.G., van den Bogaard, C., Buck, C.E., Charman, D.J., Clague, J.J., Hall, V.A., Koch, J., Mackay, H., Mallon, G., McColl, L., Pilcher, J.R., 2014. Transatlantic distribution of the Alaskan White River Ash. Geology 42, 875–878.

Kishimoto, H., Hasegawa, T., Nakagawa, M., Wada, K., 2009. Tephrostratigraphy and Eruption Style of Mashu Volcano, During the last 14,000 years, Eastern Hokkaido, Japan. Bull. Volcanol. Soc. Jpn. 54, 15–36.

Kyle, P.R., Ponomareva, V.V., Rourke Schluep, R., 2011. Geochemical characterization of marker tephra layers from major Holocene eruptions, Kamchatka Peninsula, Russia. Int. Geol. Rev. 53, 1059–1097.

Larsen, C., Newton, A.J., Dugmore, A.J., Vilmundardóttir, E.G., 2001a. Geochemistry, dispersal, volumes and chronology of Holocene from the Katla volcanic silicic tephra layers system, Iceland. J. Quat. Sci. 16, 119–132.

Larsen, G., Eiríksson, J., Knudsen, K.-L., Heinemeier, J., 2002. Correlation of late Holocene terrestrial and marine tephra markers, north Iceland: implications for reservoir age changes. Polar Res. 21, 283–290.

Larsen, G., Newton, A.J., Dugmore, A.J., Vilmundardóttir, E.G., 2001b. Geochemistry, dispersal, volumes and chronology of Holocene silicic tephra layers from the Katla volcanic system, Iceland. J. Quat. Sci. 16, 119–132.

Larsen, G., Thorarinsson, S., 1977. H4 and other acid tephra layers. Jokull 27, 28–46.

Le Maitre, R.W., 1989. A Classification of Igneous Rocks and Glossary of Terms. Blackwell Scientific Publications.

Lin, J.M., Svensson, A., Hvidberg, C.S., Lohmann, J., Kristiansen, S., Dahl-Jensen, D., Steffensen, J.P., Rasmussen, S.O., Cook, E., Kjaer, H.A., Vinther, B.M., Fischer, H., Stocker, T., Sigl, M., Bigler, M., Severi, M., Traversi, R., Mulvaney, R., 2022. Magnitude, frequency and climate forcing of global volcanism during the last glacial period as seen in Greenland and Antarctic ice cores (60-9 ka). Clim. Past 18, 485–506.

Machida, H., Arai, F., 2003. Atlas of Tephra in and Around Japan. University of Tokyo Press, Tokyo.

MacLeod, N.S., Sherrod, D.R., Chitwood, L.A., Jensen, R.A., 1995. Geologic Map of Newberry Volcano, Deschutes, Klamath, and Lake Counties, Oregon, U.S. Geological Survey Miscellaneous Investigations Series Map I-2455, 2 Sheets, Scale 1:62,500, Pamphlet. U.S. Geological Survey, p. 23.

Martin-Puertas, C., Walsh, A.A., Blockley, S.P.E., Harding, P., Biddulph, G.E., Palmer, A., Ramisch, A., Brauer, A., 2021. The first Holocene varve chronology for the UK: Based on the integration of varve counting, radiocarbon dating and tephrostratigraphy from Diss Mere (UK). Quat. Geochronol. 61, 101134.

Mayewski, P.A., Meeker, L.D., Twickler, M.S., Whitlow, S., Yang, Q., Lyons, W.B., Prentice, M., 1997. Major features and forcing of high latitudes Northern Hemisphere atmospheric circulation using a 110,000 year long glaciochemical series. J. Geophys. Res. 102, 345–365.

McConnell, J.R., Sigl, M., Plunkett, G., Burke, A., Kim, W.M., Raible, C.C., Wilson, A.I., Manning, J.G., Ludlow, F., Chellman, N.J., Innes, H.M., Yang, Z., Larsen, J.F., Schaefer, J.R., Kipfstuhl, S., Mojtabavi, S., Wilhelms, F., Opel, T., Meyer, H., Steffensen, J.P., 2020. Extreme climate after massive eruption of Alaska's Okmok volcano in 43 BCE and effects on the late Roman Republic and Ptolemaic Kingdom. Proc. Natl. Acad. Sci. USA 117, 15443–15449.

Meara, R.H., Thordarson, T., Pearce, N.J.G., Hayward, C., Larsen, G., 2020. A catalogue of major and trace element data for Icelandic Holocene silicic tephra layers. J. Quat. Sci. 35, 122–142.

Melekestsev, I.V., Braitseva, O.A., Ponomareva, V.V., Sulerzhitsky, L.D., 1998. A century of volcanic catastrophes in the Kurile-Kamchatka region in Early Holocene time. In: Dobretsov, N.L., Kovalenko, V.I. (Eds.), Global Environmental Change. Sibir' Division of RAS Publishing House, Novosibirsk, pp. 146–152 (in Russian).

Monteath, A.J., Bolton, M.S.M., Harvey, J., Seidenkrantz, M.S., Pearce, C., Jensen, B., 2023. Ultra-distal tephra deposits and Bayesian modelling constrain a variable marine radiocarbon offset in Placentia Bay, Newfoundland. Geochronology 5, 229–240.

Mortensen, A.K., Bigler, M., Grönvold, K., Steffensen, J.P., Johnsen, S.J., 2005. Volcanic ash layers from the Last Glacial Termination in the NGRIP ice core. J. Quat. Sci. 20, 209–219.

Mulliken, K., 2016. Holocene Volcanism and Human Occupation in the Middle Susitna River Valley, Alaska. University of Alaska Fairbanks, Fairbanks, AK. Unpublished MA thesis.

NGRIP members, 2004. High-resolution record of Northern Hemisphere climate extending into the last interglacial period. Nature 431, 147–151.

Óladóttir, B.A., Larsen, G., Sigmarsson, O., 2011a. Holocene volcanic activity at Grimsvötn, Bardarbunga and Kverkfjöll subglacial centres beneath Vatnajökull, Iceland. Bull. Volcanol. 73, 1187–1208.

Óladóttir, B.A., Larsen, G., Thordarson, T., Sigmarsson, O., 2005. The Katla volcano S-Iceland: Holocene tephra stratigraphy and eruption frequency. Jokull 55, 53–74.

Óladóttir, B.A., Sigmarsson, O., Larsen, G., Devidal, J.L., 2011b. Provenance of basaltic tephra from Vatnajökull subglacial volcanoes, Iceland, as determined by major- and trace-element analyses. Holocene 21, 1037–1048.

Óladóttir, B.A., Sigmarsson, O., Larsen, G., Thordarson, T., 2008. Katla volcano, Iceland: magma composition, dynamics and eruption frequency as recorded by Holocene tephra layers. Bull. Volcanol. 70, 475–493.

Palais, J.M., Germani, M.S., Zielinski, G.A., 1992. Interhemispheric transport of volcanic ash from a 1259 A. D. volcanic eruption to the Greenland and Antarctic ice sheets. Geophys. Res. Lett. 19, 801–804.

Palais, J.M., Taylor, K., Mayewski, P.A., Grootes, P., 1991. Volcanic Ash from the 1362 A. D. Oraefajökull Eruption (Iceland) in the Greenland Ice-Sheet. Geophys. Res. Lett. 18, 1241–1244.

Pearson, C., Sigl, M., Burke, A., Davies, S., Kurbatov, A., Severi, M., Cole-Dai, J., Innes, H., Albert, P.G., Helmick, M., 2022. Geochemical ice-core constraints on the timing and climatic impact of Aniakchak II (1628 BCE) and Thera (Minoan) volcanic eruptions. PNAS Nexus 1, 1–12.

Peccerillo, A., Taylor, S.R., 1976. Geochemistry of eocene calc-alkaline volcanic rocks from the Kastamonu area, Northern Turkey. Contrib. Mineral. Petrol. 58, 63–81.

Pendea, I.F., Ponomareva, V., Bourgeois, J., Zubrow, E.B.W., Portnyagin, M., Ponkratova, I., Harmsen, H., Korosec, G., 2017. Late Glacial to Holocene paleoenvironmental change on the northwestern Pacific seaboard, Kamchatka Peninsula (Russia). Quat. Sci. Rev. 157, 14–28.

Pilcher, J., Bradley, R.S., Francus, P., Anderson, L., 2005. A Holocene tephra record from the Lofoten Islands, Arctic Norway. Boreas 34, 136–156.

Pilcher, J.R., Hall, V.A., 1996. Tephrochronological studies in northern England. Holocene 6, 100–105.

Pilcher, J.R., Hall, V.A., McCormac, F.G., 1995. Dates of Icelandic volcanic eruptions from tephra layers in Irish peats. Holocene 5, 103–110.

Pilcher, J.R., Hall, V.A., McCormac, F.G., 1996. An outline tephrochronology for the Holocene of the north of Ireland. J. Quat. Sci. 11, 485–494.

Plunkett, G., Coulter, S.E., Ponomareva, V.V., Blaauw, M., Klimaschewski, A., Hammarlund, D., 2015. Distal tephrochronology in volcanic regions: Challenges and insights from Kamchatkan lake sediments. Global Planet. Change 134, 26–40.

Plunkett, G., Pilcher, J.R., 2018. Defining the potential source region of volcanic ash in northwest Europe during the Mid- to Late Holocene. Earth Sci. Rev. 179, 20–37.

Plunkett, G., Sigl, M., McConnell, J.R., Pilcher, J.R., Chellman, N.J., 2023. The significance of volcanic ash in Greenland ice cores during the Common Era. Quat. Sci. Rev. 301.

Plunkett, G.M., Pilcher, J.R., McCormac, F.G., Hall, V.A., 2004. New dates for first millennium BC tephra isochrones in Ireland. Holocene 14, 780–786.

Ponomareva, V., Portnyagin, M., Pendea, I.F., Zelenin, E., Bourgeois, J., Pinegina, T., Kozhurin, A., 2017. A full holocene tephrochronology for the Kamchatsky Peninsula region: Applications from Kamchatka to North America. Quat. Sci. Rev. 168, 101–122.

Ponomareva, V.V., Kyle, P.R., Melekestsev, I.V., Rinkleff, P.G., Dirksen, O.V., Sulerzhitsky, L.D., Zaretskaia, N.E., Rourke, R., 2004. The 7600 (^{14}C) year BP Kurile Lake caldera-forming eruption, Kamchatka, Russia: stratigraphy and field relationships. J. Volcanol. Geoth. Res. 136, 199–222.

Portnyagin, M.V., Ponomareva, V.V., Zelenin, E.A., Bazanova, L.I., Pevzner, M.M., Plechova, A.A., Rogozin, A.N., Garbe-Schönberg, D., 2020. TephraKam: geochemical database of glass compositions in tephra and welded tuffs from the Kamchatka volcanic arc (northwestern Pacific). Earth Syst. Sci. Data 12, 469–486.

Pyle, D.M., 2000. Sizes of volcanic eruptions. In: Sigurdsson, H., Houghton, B., S, M. (Eds.), The Encyclopedia of Volcanoes. Academic Press, pp. 257–264.

Pyne-O'Donnell, S.D.F., Hughes, P.D.M., Froese, D.G., Jensen, B.J.L., Kuehn, S.C., Mallon, G., Amesbury, M.J., Charman, D.J., Daley, T.J., Loader, N.J., Mauquoy, D., Street-Perrott, F.A., Woodman-Ralph, J., 2012. High-precision ultra-distal Holocene tephrochronology in North America. Quat. Sci. Rev. 52, 6–11.

Ramsey, C.B., Lee, S., 2013. Recent and Planned Developments of the Program OxCal. Radiocarbon 55, 720–730.

Razzhigaeva, N.G., Matsumoto, A., Nakagawa, M., 2016. Age, source, and distribution of Holocene tephra in the southern Kurile Islands: Evaluation of Holocene eruptive activities in the southern Kurile arc. Quat. Int. 397, 63–78.

Reimer, P.J., Austin, W.E.N., Bard, E., Bayliss, A., Blackwell, P.G., Bronk Ramsey, C., Butzin, M., Cheng, H., Edwards, R.L., Friedrich, M., Grootes, P.M., Guilderson, T.P., Hajdas, I., Heaton, T.J., Hogg, A.G., Hughen, K.A., Kromer, B., Manning, S.W., Muscheler, R., Palmer, J.G., Pearson, C., van der Plicht, J., Reimer, R.W., Richards, D.A., Scott, E.M., Southon, J.R., Turney, C.S.M., Wacker, L., Adolphi, F., Büntgen, U., Capano, M., Fahrni, S.M., Fogtmann-Schulz, A., Friedrich, R., Köhler, P., Kudsk, S., Miyake, F., Olsen, J., Reinig, F., Sakamoto, M., Sookdeo, A., Talamo, S., 2020. The IntCal20 Northern Hemisphere Radiocarbon Age Calibration Curve (0–55 cal kBP). Radiocarbon 62, 725–757.

Riehle, J.R., 1985. A reconnaissance of the major Holocene tephra deposits in the upper Cook Inlet region, Alaska. J. Volcanol. Geoth. Res. 26, 37–74.

Roland, T.P., Caseldine, C.J., Charman, D.J., Turney, C.S.M., Amesbury, M.J., 2014. Was there a '4.2 ka event' in Great Britain and Ireland? Evidence from the peatland record. Quat. Sci. Rev. 83, 11–27.

Schiff, C.J., Kaufman, D.S., Wallace, K.L., Ketterer, M.E., 2010. An improved proximal tephrochronology for Redoubt Volcano, Alaska. J. Volcanol. Geoth. Res. 193, 203–214.

Self, S., Gertisser, R., 2015. Tying down eruption risk. Nat. Geosci. 8, 248–250.

Sigl, M., Toohey, M., McConnell, J.R., Cole-Dai, J., Severi, M., 2022. Volcanic stratospheric sulfur injections and aerosol optical depth during the Holocene (past 11500 years) from a bipolar ice-core array. Earth Syst. Sci. Data 14, 3167–3196.

Sigl, M., Winstrup, M., McConnell, J.R., Welten, K.C., Plunkett, G., Ludlow, F., Buntgen, U., Caffee, M., Chellman, N., Dahl-Jensen, D., Fischer, H., Kipfstuhl, S., Kostick, C., Maselli, O.J., Mekhaldi, F., Mulvaney, R., Muscheler, R., Pasteris, D.R., Pilcher, J.R., Salzer, M., Schupbach, S., Steffensen, J.P., Vinther, B.M., Woodruff, T. E., 2015. Timing and climate forcing of volcanic eruptions for the past 2,500 years. Nature 523, 543–549.

Smith, V.C., Costa, A., Aguirre-Díaz, G., Pedrazzi, D., Scifo, A., Plunkett, G., Poret, M., Tournigand, P.Y., Miles, D., Dee, M.W., McConnell, J.R., Sunyé-Puchol, I., Harris, P.

D., Sigl, M., Pilcher, J.R., Chellman, N., Gutiérrez, E., 2020. The magnitude and impact of the 431 CE Tierra Blanca Joven eruption of Ilopango, El Salvador. Proc. Natl. Acad. Sci. U.S.A. 117, 26061–26068.

Smith, V.C., Staff, R.A., Blockley, S.P.E., Bronk Ramsey, C., Nakagawa, T., Mark, D.F., Takemura, K., Danhara, T., 2013. Identification and correlation of visible tephras in the Lake Suigetsu SG06 sedimentary archive, Japan: chronostratigraphic markers for synchronising of east Asian/west Pacific palaeoclimatic records across the last 150 ka. Quat. Sci. Rev. 67, 121–137.

Spano, N.G., Lane, C.S., Francis, S.W., Johnson, T.C., 2017. Discovery of Mount Mazama cryptotephra in Lake Superior (North America): Implications and potential applications. Geology 45, 1071–1074.

Stevenson, J.A., Larsen, G., Thordarson, T., 2015. Physical Volcanology of the Prehistoric Hekla 3 and Hekla 4 Eruptions, Iceland. In: Conference Abstract, EGU General Assembly 12-17 April 2015. Vienna, Austria. id.4207.

Sun, C., Plunkett, G., Liu, J., Zhao, H., Sigl, M., McConnell, J.R., Pilcher, J.R., Vinther, B., Steffensen, J.P., Hall, V., 2014. Ash from Changbaishan Millennium eruption recorded in Greenland ice: Implications for determining the eruption's timing and impact. Geophys. Res. Lett. 41, 694–701.

Svensson, A., Dahl-Jensen, D., Steffensen, J.P., Blunier, T., Rasmussen, S.O., Vinther, B. M., Vallelonga, P., Capron, E., Gkinis, V., Cook, E., Kjaer, H.A., Muscheler, R., Kipfstuhl, S., Wilhelms, F., Stocker, T.F., Fischer, H., Adolphi, F., Erhardt, T., Sigl, M., Landais, A., Parrenin, F., Buizert, C., McConnell, J.R., Severi, M., Mulvaney, R., Bigler, M., 2020. Bipolar volcanic synchronization of abrupt climate change in Greenland and Antarctic ice cores during the last glacial period. Clim. Past 16, 1565–1580.

Sverrisdóttir, G., 2007. Hybrid magma generation preceding Plinian silicic eruptions at Hekla, Iceland: evidence from mineralogy and chemistry of two zoned deposits. Geol. Mag. 144, 643–659.

Swindles, G.T., 2006. Reconstructions of Holocene Climate Change from Peatland in the North of Ireland. Queen's University Belfast. Unpublished PhD thesis.

Thorarinsson, S., 1971. The age of the light Hekla tephra layers according to corrected 14C datings. Náttúrufrœðingurinn 41, 99–105.

Tomlinson, E.L., Thordarson, T., Müller, W., Thirlwall, M., Menzies, M.A., 2010. Microanalysis of tephra by LA-ICP-MS — Strategies, advantages and limitations assessed using the Thorsmörk ignimbrite (Southern Iceland). Chem. Geol. 279, 73–89.

Toohey, M., Sigl, M., 2017. Volcanic stratospheric sulfur injections and aerosol optical depth from 500 BCE to 1900 CE. Earth Syst. Sci. Data 9, 809–831.

van den Bogaard, C., Schmincke, H.-U., 2002. Linking the North Atlantic to central Europe: a high resolution Holocene tephrochronological record from northern Germany. J. Quat. Sci. 17, 3–20.

van der Bilt, W.G.M., Lane, C.S., Bakke, J., 2017. Ultra-distal Kamchatkan ash on Arctic Svalbard: Towards hemispheric cryptotephra correlation. Quat. Sci. Rev. 164, 230–235.

Veres, D., Bazin, L., Landais, A., Toyé Mahamadou Kele, H., Lemieux-Dudon, B., Parrenin, F., Martinerie, P., Blayo, E., Blunier, T., Capron, E., Chappellaz, J., Rasmussen, S.O., Severi, M., Svensson, A., Vinther, B., Wolff, E.W., 2013. The Antarctic ice core chronology (AICC2012): an optimized multi-parameter and multi-site dating approach for the last 120 thousand years. Clim. Past 9, 1733–1748.

Vinther, B.M., Clausen, H.B., Johnsen, S.J., Rasmussen, S.O., Andersen, K.K., Buchardt, S. L., Dahl-Jensen, D., Seierstad, I.K., Siggaard-Andersen, M.L., Steffensen, J.P., Svensson, A., Olsen, J., Heinemeier, J., 2006. A synchronized dating of three Greenland ice cores throughout the Holocene. J. Geophys. Res.: Atmosphere 111, D13102.

Volynets, O.N., Ponomareva, V.V., Braitseva, O.A., Melekestsev, I.V., Chen, C.H., 1999. Holocene eruptive history of Ksudach volcanic massif, South Kamchatka: evolution of a large magmatic chamber. J. Volcanol. Geoth. Res. 91, 23–42.

Vorren, K.-D., Blaauw, M., Wastegård, S., Plicht, J.V.d., Jensen, C., 2007. High-resolution stratigraphy of the northernmost concentric raised bog in Europe: Sellevollmyra, Andøya, northern Norway. Boreas 36, 253–277.

Walsh, A.A., Blockley, S.P.E., Milner, A.M., Martin-Puertas, C., 2023. Updated age constraints on key tephra markers for NW Europe based on a high-precision varve lake chronology. Quat. Sci. Rev. 300, 107897.

Walsh, A.A., Blockley, S.P.E., Milner, A.M., Matthews, I.P., Martin-Puertas, C., 2021. Complexities in European Holocene cryptotephra dispersal revealed in the annually laminated lake record of Diss Mere, East Anglia. Quat. Geochronol. 66, 101213.

Wastegård, S., 2005. Late Quaternary tephrochronology of Sweden: a review. Quat. Int. 130, 49–62.

Wastegård, S., Björck, S., Grauert, M., Hannon, G.E., 2001. The Mjáuvøtn tephra and other Holocene tephra horizons from the Faroe Islands: a link between the Icelandic source region, the Nordic Seas and the European continent. Holocene 11, 101–109.

Wastegård, S., Rundgren, M., Schoning, K., Andersson, S., Björck, S., Borgmark, A., Possnert, G., 2008. Age, geochemistry and distribution of the mid-Holocene Hekla-S/ Kebister tephra. Holocene 18, 539–549.

Watson, E.J., Swindles, G.T., Lawson, I.T., Savov, I.P., 2016. Do peatlands or lakes provide the most comprehensive distal tephra records? Quat. Sci. Rev. 139, 110–128.

Wulf, S., Dräger, N., Ott, F., Serb, J., Appelt, O., Guðmundsdóttir, E., van den Bogaard, C., Słowiński, M., Błaszkiewicz, M., Brauer, A., 2016. Holocene tephrostratigraphy of varved sediment records from Lakes Tiefer See (NE Germany) and Czechowskie (N Poland). Quat. Sci. Rev. 132, 1–14.

Yamamoto, T., Itho, J.-i., Nakagawa, M., Hasegawa, T., Kishimoto, H., 2010. 14C ages for the ejecta from Kutcharo and Mashu calderas, eastern Hokkaido, Japan. Bull. Geol. Surv. Jpn. 61, 161–170.

Young, S.R., 1990. Physical Volcanology of Holocene Airfall Deposits from Mt Mazama, Crater Lake, Oregon. University of Lancaster.

Zdanowicz, C.M., Zielinski, G.A., Germani, M.S., 1999. Mount Mazama eruption: Calendrical age verified and atmospheric impact assessed. Geology 27, 621–624.

Zielinski, G.A., 1995. Stratospheric loading and optical depth estimates of explosive volcanism over the last 2100 years derived from the GISP2 Greenland ice core. J. Geophys. Res. 100 (D10) 20,937-, 20,955.

Zielinski, G.A., Mayewski, P.A., Meeker, L.D., Grönvold, K., Germani, M.S., Whitlow, S., Twickler, M.S., Taylor, K., 1997. Volcanic aerosol records and tephrochronology of the Summit, Greenland, ice cores. J. Geophys. Res. 102 (26), 625–626, 640.

Zillén, L.M., Wastegård, S., Snowball, I.F., 2002. Calendar year ages of three mid-Holocene tephra layers identified in varved lake sediment in west central Sweden. Quat. Sci. Rev. 21, 1583–1591.